

---

# Random-Set Neural Networks (RS-NN)

---

Shireen Kudukkil Manchingal<sup>1\*</sup> Muhammad Mubashar<sup>1</sup> Kaizheng Wang<sup>2</sup>  
Keivan Shariatmadar<sup>3</sup> Fabio Cuzzolin<sup>1</sup>

<sup>1</sup>Visual Artificial Intelligence Laboratory (VAIL), Oxford Brookes University

<sup>1</sup>KU Leuven, Department of Computer Science,

<sup>3</sup>KU Leuven, Department of Mechanical Engineering,  
{s.manchingal, 19230664, fabio.cuzzolin}@brookes.ac.uk  
{kaizheng.wang, keivan.shariatmadar}@kuleuven.be

## Abstract

Machine learning is increasingly deployed in safety-critical domains where robustness against adversarial attacks is crucial and erroneous predictions could lead to potentially catastrophic consequences. This highlights the need for learning systems to be equipped with the means to determine a model’s confidence in its prediction and the epistemic uncertainty associated with it, ‘to know when a model does not know’. In this paper, we propose a novel Random-Set Neural Network (RS-NN) for classification. RS-NN predicts belief functions rather than probability vectors over a set of classes using the mathematics of *random sets*, i.e., distributions over the power set of the sample space. RS-NN encodes the ‘epistemic’ uncertainty induced in machine learning by limited training sets via the size of the credal sets associated with the predicted belief functions. Our approach outperforms state-of-the-art Bayesian (LB-BNN, BNN-R) and Ensemble (ENN) methods in a classical evaluation setting in terms of performance, uncertainty estimation and out-of-distribution (OoD) detection on several benchmarks (CIFAR-10 vs SVHN/Intel-Image, MNIST vs FMNIST/KMNIST, ImageNet vs ImageNet-O) and scales effectively to large-scale architectures such as WideResNet-28-10, VGG16, Inception V3, EfficientNetB2, and ViT-Base.

## 1 Introduction

Despite its success, artificial intelligence, in its current form, struggles to provide reliable predictions when confronted with unfamiliar data [45]. This includes noisy samples [86] deliberately designed to deceive models, or out-of-distribution data (OoD) beyond the model’s training distribution. This emphasizes the need for learning systems to be able to determine a model’s confidence in its own predictions, acknowledge the limits of its knowledge and gauge these limitations to make informed decisions by modelling the *epistemic uncertainty* associated with it, in essence, ‘to know when a model does not know’. Epistemic uncertainty pertains to uncertainty associated with our ignorance about the underlying data generation process [56, 53, 70]. Within machine learning, a major source of epistemic uncertainty arises from the limited representativeness of the available training data, constrained in both quantity and quality.

In this paper, we propose to model epistemic uncertainty using a *random set* approach [74]. As we focus on classification involving a finite list of classes, we model uncertainty using *belief functions* [93], the finite incarnation of random sets [20]. The theory of belief functions, or Dempster-Shafer theory of evidence [93], is, in fact, a generalisation of Bayesian inference [97]. Classical (discrete) probabilities are simply special belief functions, and Bayes’ rule is a special case of Dempster’s rule originally proposed for the combination of belief functions. Fig. 1 contrasts the inference processes of a Random-Set Neural Network (RS-NN) and a Bayesian Neural Network [55]. In hierarchical

---

\*Corresponding author.

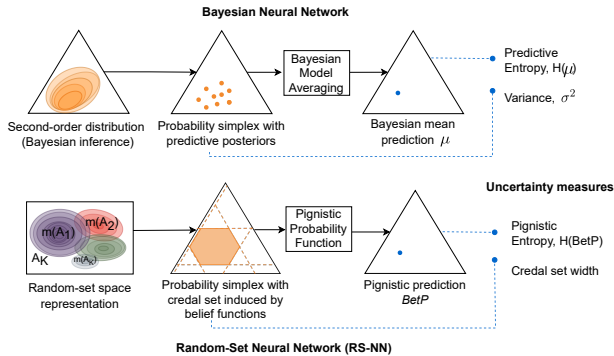


Figure 1: Inference in a Bayesian Neural Network (top) as opposed to a Random-Set Neural Network (bottom), with corresponding measures of uncertainty and their sources.

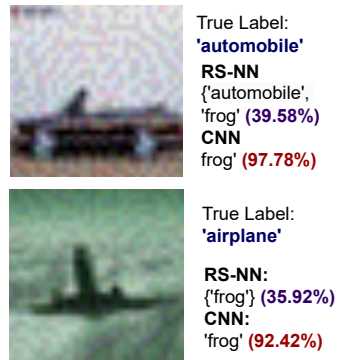


Figure 2: Confidence scores of RS-NN and CNN for FGSM attack ( $\epsilon = 0.05$ ) on CIFAR-10.

Bayesian inference, the predictive posterior distribution is a second-order probability distribution [53]. It involves sampling from predicted first-order distributions for a collection of possible models within the Bayesian Neural Network. A single (mean) prediction is derived by Bayesian Model Averaging (BMA), while uncertainty is measured by the entropy of the mean prediction and the variance of the posterior distributions.

In a Random-Set NN (RS-NN) (Fig. 1, bottom), each test input at inference time is mapped to a belief function [93] on the collection of classes  $\mathcal{C}$ . This belief function is encoded by a mass value  $m(A) \in [0, 1]$  assigned to a finite budget  $\mathcal{O} = \{A_k \subset \mathcal{C}\}$  of sets of classes. The most relevant such sets are identified from training data by fitting Gaussian Mixture Models (GMMs) to the labelled data and computing the overlap among the resulting clusters [99]. Such a predicted belief function is mathematically equivalent to a convex set of probability vectors (a *credal set* [68, 18]) on the class list  $\mathcal{C}$ . A pointwise prediction can then be obtained by computing the centre of mass of this credal set, termed *pignistic probability* [98]. In RS-NN, uncertainty can be expressed either via the entropy of the pignistic prediction, or via the width of the credal set prediction [6]. As we show in this paper, the entropy of a pignistic prediction is more diverse than that of a Bayesian prediction across in-distribution and out-of-distribution data (see Tab. 1), and the width of the credal prediction, as it encodes epistemic uncertainty about the prediction itself, is empirically much less correlated with the confidence score than entropy (see §D.5.1).

Using a random-set representation prevents the need to discard information, a challenge observed in Bayesian Model Averaging [50, 44]. While Bayesian inference requires defining prior distributions for model parameters even in the absence of relevant information, in belief theory, priors are not required for the inference process, thus avoiding the selection bias risks that can seriously condition Bayesian reasoning [35]. Based on our extensive experiments on multiple datasets, including large-scale ones, RS-NNs not only demonstrate superior accuracy compared to state-of-the-art Bayesian models (Sec. 4.2), but also arguably better encode the epistemic uncertainty associated with the predictions (Sec. 4.4) and better distinguish between in-distribution and out-of-distribution data (Sec. 4.3). Furthermore, RS-NNs effectively circumvent the tendency of standard neural networks to generate overconfident incorrect predictions, as illustrated in Fig. 2 in an experiment on Fast Gradient Sign Method (FGSM) [43] adversarial attacks on CIFAR-10. CNN misclassifies with high confidence scores of 92.42% and 97.78%, while RS-NN shows lower confidence at 35.92% and 39.58%.

**Contributions.** **Firstly**, we propose a novel *Random-Set Neural Network (RS-NN)* based on the principle that a deep neural network predicting belief values for sets of classes, rather than individual classes, has the potential to be a more faithful representation of the epistemic uncertainty induced by the limited quantity and quality of the training data. As they assign probability values to sets of outcomes directly, random sets [75, 74] naturally model the fact that observations almost invariably come in the form of sets, and can accommodate ambiguity, incomplete data, and non-probabilistic uncertainties. **Secondly**, we develop a novel *budgeting* method for efficiently selecting from the training data a fixed budget of relevant sets of classes for the task at hand, by fitting Gaussian Mixture Models to classes and computing clusters of classes, thus avoiding the exponential complexity of vanilla random-set implementations and ensuring scalability. A random-set representation serves as a

foundational framework: when integrated with a budgeting of sets, this method acts as a versatile wrapper applicable to any model architecture. **Thirdly**, we illustrate the advantages of two new methods for assessing the uncertainty associated with a random-set prediction: the Shannon entropy of the pignistic prediction (the centre of mass of the corresponding credal set) and the width of the credal prediction itself. **Finally**, we present a large body of experimental results demonstrating how RS-NN outperforms both state-of-the-art Bayesian (BNN-R, LB-BNN) and Ensemble (ENN) methods in terms of: (i) performance (test accuracy, inference time) (Sec. 4.2); (ii) results on various out-of-distribution (OoD) benchmarks (Sec. 4.3), including CIFAR-10 vs. SVHN/Intel-Image, MNIST vs. FMNIST/KMNIST, and ImageNet vs. ImageNet-O; (iii) ability to provide reliable measures of uncertainty quantification (Sec. 4.4) in the form of pignistic entropy and credal set width, verified on OoD benchmarks; (iv) scalability to large-scale architectures (WideResNet-28-10, Inception V3, EfficientNet B2, ViT-Base) and datasets (e.g. ImageNet) (Sec. 4.5). Additionally, we provide statistical guarantees on RS-NN using non-conformity scores (§A), we show how RS-NN is robust to adversarial attacks (§D.2) and noisy data (§D.1), and circumvents the overconfidence problem in CNNs (§D.3). A qualitative assessment of entropy vs credal set width is given in §D.5.1.

**Paper outline.** We first recall the notion of random sets, the mathematics of belief functions, and the associated credal and pignistic predictions (Sec. 2). We then explain the architecture, loss function and uncertainty representation of RS-NN (Sec. 3). In Sec. 4, we provide a large body of evidence supporting our approach. Sec. 4.6 details the limitations our method, including the budgeting time and fixed number of focal sets. Finally, Sec. 5 concludes and outlines future work. Appendix §A includes a discussion on statistical guarantees, §B, §C and §D contain additional evidence.

**Related Work.** The machine learning community has recognised the challenge of estimating uncertainty in model predictions, leading to the development of various methods such as Bayesian approximations [38], evidential Dirichlet distributions [92] and conformal prediction [94, 83, 8, 105, 3]. Some methods rely on prior knowledge [34], whereas others require setting a desired threshold on the metrics [3]. Some [11, 53] argued that classical probability theory is, in fact, not equipped to model “second-level” uncertainty on the probabilities themselves. This has led to the formulation of numerous uncertainty calculi [21], including possibility theory [30], probability intervals [47], credal sets [68], random sets [79] and imprecise probability [109].

Bayesian approaches, pioneered by Buntine [12] and others [69, 77], have recently become dominant in uncertainty estimation. Notable techniques include R-BNN (Reparameterisation) [60], variational inference with reparameterisation trick and Laplace Bridge Bayesian approximation (LB-BNN) [51] which uses the Laplace Bridge to map efficiently between Gaussian and Dirichlet distributions and enhance computational efficiency. Various approximations of full Bayesian inference exist, such as Markov chain Monte Carlo (MCMC), variational inference (VI), and Dropout Variational Inference [37]. Recent work addresses challenges in computational cost, model priors, and tractable function-space variational inference [52, 22, 102, 89]. Despite their advantages, Bayesian models face challenges when the model prior is misspecified. Our approach mitigates these challenges by eliminating the need for sampling during inference and prior selection, reducing computational complexity compared to Bayesian inference, as demonstrated in our experiments (see Tab. 2). Ensemble-based approaches, such as Deep Ensembles [66] and Epistemic Neural Networks (ENN) [82], efficiently estimate uncertainty by leveraging multiple models. However, the computational cost of training ensembles, especially for large models, is often impractical (see Appendix §B).

## 2 Random sets and belief functions

**Random sets.** A die is a simple example of a (discrete) random variable. Its probability space is defined on the sample space  $\Theta = \{\text{face 1, face 2, } \dots, \text{face 6}\}$ , where elements are mapped to the real numbers  $1, 2, \dots, 6$ , respectively. Now, imagine that faces 1 and 2 are cloaked, and we roll the die. How do we model this new experiment, mathematically? Actually, the probability space has not changed (as the physical die has not been altered, its faces still have the same probabilities). What has changed is the mapping: since we cannot observe the outcome when a cloaked face is shown (we assume that only the top face is observable), both face 1 and face 2 (as elements of  $\Theta$ ) are mapped to the set of possible values  $\{1, 2\}$  on the real line  $\mathbb{R}$  (Fig. 3). Mathematically, this is a *random set* [73, 57, 79, 75], i.e., a set-valued random variable, modelling random experiments in which observations come in the form of sets.

**Belief functions.** Random sets have been proposed by Dempster [23] and later Shafer [93] as a mathematical model for subjective belief, alternative to Bayesian probability. For this reason, on

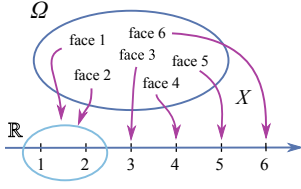


Figure 3: The random set (set-valued random variable) associated with a cloaked die in which faces 1 and 2 are not visible.

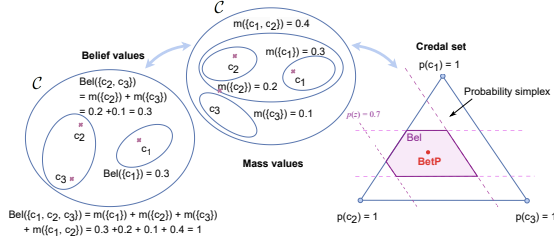


Figure 4: A belief function is equivalent to a credal set with boundaries determined by lower bounds (4) on probability values.

finite domains (classification) they assume the name of *belief functions*. While classical discrete mass functions assign normalised, non-negative values to *elements*  $\theta \in \Theta$  of their sample space, a belief function independently assigns normalised, non-negative mass values to *subsets* of the sample space:

$$m(A) \geq 0, \forall A \subset \Theta, \sum_A m(A) = 1. \quad (1)$$

The belief function associated with a mass function  $m$  then measures the total mass of the subsets of each focal set  $A$ . Mass functions can be recovered from belief functions via Moebius inversion [93]:

$$Bel(A) = \sum_{B \subseteq A} m(B), \quad m(A) = \sum_{B \subseteq A} (-1)^{|A \setminus B|} Bel(B). \quad (2)$$

It follows that classical (discrete) probability measures are a special case of belief functions. Consider for instance a sample space (class list)  $\Theta = \mathcal{C} = \{c_1, c_2, c_3\}$  and let  $2^\Theta$  be its power set (collection of all subsets). Define a mass function  $m : 2^\Theta \rightarrow [0, 1]$  as:  $m(\{c_1\}) = 0.3$ ,  $m(\{c_2\}) = 0.2$ ,  $m(\{c_3\}) = 0.1$ ,  $m(\{c_1, c_2\}) = 0.4$ , whereas  $m(\{c_1, c_3\}) = 0$ ,  $m(\{c_2, c_3\}) = 0$  and  $m(\{c_1, c_2, c_3\}) = 0$  (Fig. 4, top). Note that  $m$  is normalised:  $\sum_{B \subseteq \Theta} m(B) = 1$ . By (2), the belief value of the composite class  $\{c_2, c_3\}$  is:  $Bel(\{c_2, c_3\}) = m(\{c_2\}) + m(\{c_3\}) = 0.2 + 0.1 = 0.3$  (Fig. 4, left). Similarly, the belief value of composite class  $\{c_1, c_2\}$  can be computed as  $Bel(\{c_1, c_2\}) = m(\{c_1\}) + m(\{c_2\}) + m(\{c_1, c_2\}) = 0.3 + 0.2 + 0.4 = 0.9$ .

**Pignistic probability.** Given a belief function  $Bel$ , its *pignistic probability* is the precise probability distribution obtained by re-distributing the mass of its focal sets  $A$  to its constituent elements,  $c \in A$ :

$$BetP(c) = \sum_{A \ni c} \frac{m(A)}{|A|}. \quad (3)$$

Smets [95] originally proposed to use the pignistic probability for decision making using belief functions, by applying expected utility to it. Notably, the pignistic probability is geometrically the centre of mass of the credal set associated with a belief function ([20], Fig. 4).

**Credal prediction.** As anticipated, RS-NN is designed to predict a belief function (a finite random set) on the set of classes. A belief function, in turn, is associated with a convex set of probability distributions (a *credal set* [68, 114, 19, 7, 6, 18]) on the same domain. This is the set:

$$Cre = \{P : \mathcal{C} \rightarrow [0, 1] | Bel(A) \leq P(A)\}, \quad (4)$$

where  $P$  is any probability distribution on the collection of classes  $\mathcal{C}$ . As they have belief values as lower bounds, credal sets induced by belief functions have a peculiar shape (see Fig. 4, right, for a case with 3 classes). Their vertices are induced by the permutations of the elements of the sample space (for us, the set of classes) [14, 18]. Given one such permutation (e.g.,  $(c_2, c_4, c_1, c_3)$  for a set of 4 classes) the probability vector representing the corresponding vertex of the credal prediction assigns to each specific class the mass of all the focal sets containing that class, *but* not containing any class preceding it in the permutation order [110].

The size of the resulting credal prediction measures the extent of the related epistemic uncertainty (see Sec. 3.3), arising from lack of evidence. A credal prediction, by encompassing multiple potential distributions, reflects the model's acknowledgment of this uncertainty. A wider credal set indicates higher uncertainty, as the model refrains from committing to a specific probability distribution due to limited or conflicting evidence. In contrast, a narrower credal set implies lower uncertainty, signifying a more confident prediction based on substantial, consistent evidence.

### 3 Random-Set Neural Network

#### 3.1 Architecture

**Representation.** A classifier  $e$  (e.g., a neural network) is a mapping from an input space  $X$  to a target space  $\mathcal{C}$  (the set of classes), i.e.,  $e : X \rightarrow \mathcal{C}$ . In our set-valued classification setting, on the other hand,  $e$  is a mapping from  $X$  to the set of all *subsets* of  $\mathcal{C}$ , the powerset  $\mathbb{P}(\mathcal{C})$ , namely:  $e : X \rightarrow \mathbb{P}(\mathcal{C})$ .

As shown in Fig. 5, RS-NN predicts for each input data point a belief function, rather than a vector of softmax probabilities as in a traditional CNN. For  $N$  classes, a ‘vanilla’ RS-NN would have  $2^N$  outputs (as  $2^N$  is the cardinality of  $\mathbb{P}(\mathcal{C})$ ), each being the belief value (2) of the focal set of classes  $A \in \mathbb{P}(\mathcal{C})$  corresponding to that output neuron. Given a training datapoint with attached a true class, its ground truth is encoded by the vector  $\mathbf{bel} = \{Bel(A), A \in \mathbb{P}(\mathcal{C})\}$  of belief values for each focal set of classes  $A \in \mathbb{P}(\mathcal{C})$ , where  $Bel(A)$  is set to 1 iff the true class is contained in the subset  $A$ , 0 otherwise.<sup>2</sup> This corresponds to full certainty that the element belongs to that set and there is complete confidence in this proposition.

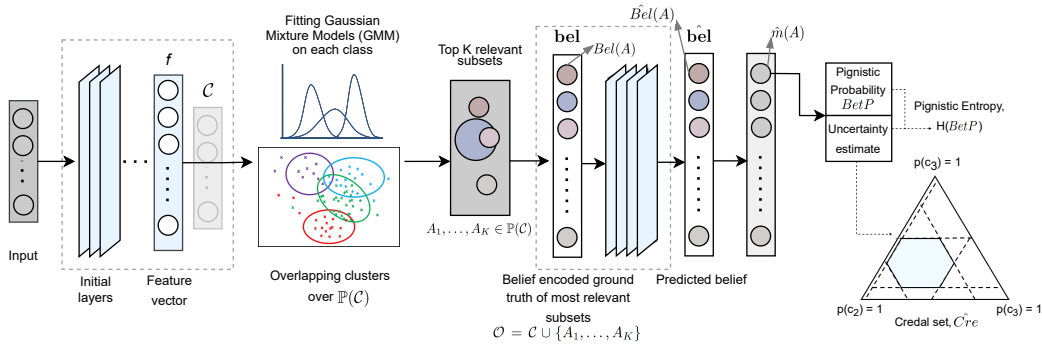


Figure 5: RS-NN model architecture. Given a collection  $\mathcal{C}$  of  $N$  classes, the network selects the top  $K$  relevant (focal) sets of classes  $A_1, \dots, A_K$  from the powerset  $\mathbb{P}(\mathcal{C})$ , encodes the ground truth training classes as belief functions  $Bel$ , and uses them to predict a belief function  $\hat{bel}$  for each input test data point, using the loss (7). Mass values  $\hat{m}$  and pignistic probability estimates  $BetP$  are computed from the predicted belief function. Uncertainty is estimated as described in Sec. 3.3

**Budgeting.** To overcome the exponential complexity of using  $2^N$  sets of classes (especially for large  $N$ ), a fixed budget of  $K$  relevant non-singleton (of cardinality  $> 1$ ) focal sets are used. These focal sets are obtained by clustering the original classes  $\mathcal{C}$  and selecting the top  $K$  focal sets of classes with the highest overlap ratio, computed as the intersection over union for each subset  $A$  in  $\mathbb{P}(\mathcal{C})$ :  $overlap(A) = \frac{\cap_{c \in A} A^c}{\cup_{c \in A} A^c}$ ,  $A_1, \dots, A_K \in \mathbb{P}(\mathcal{C})$ . The clustering is performed on feature vectors of images of each class generated by a standard CNN trained on the original classes  $\mathcal{C}$ . The feature vectors are further reduced to 3 dimensions using t-SNE (t-Distributed Stochastic Neighbor Embedding) [103] before applying a Gaussian Mixture Model (GMM) to them. Ellipsoids [99], covering 95% of data, are generated using eigenvectors and eigenvalues of the covariance matrix  $\Sigma_c$  and the mean vector  $\mu_c$ ,  $\forall c \in \mathcal{C}$ ,  $P_c \sim \mathcal{N}(x_c; \mu_c, \Sigma_c)$  obtained from the GMM to calculate the overlaps. To avoid computing a degree of overlap for all  $2^N$  subsets, the algorithm is early stopped when increasing the cardinality does not alter the list of most-overlapping sets of classes.

The  $K$  non-singleton focal sets so obtained, along with the  $N$  original (singleton) classes, form our network outputs  $\mathcal{O} = \mathcal{C} \cup \{A_1, \dots, A_K\}$ . E.g., in a 100-class scenario, the powerset contains  $2^{100}$  subsets ( $10^{30}$  possibilities). Setting a budget of  $K = 200$ , for instance, results in  $100 + K = 300$  outputs, a far more manageable number.

The budgeting step is a one-time procedure, applied to any given dataset before training. It requires just 2 minutes for CIFAR-10, 7 minutes for CIFAR-100, and 2 hours for ImageNet ( $\approx 1.1M$  images, 1000 classes). In return, it greatly helps overcome the computational challenge of dealing with a large number of classes. Budgeting can be performed on features obtained from pre-trained classifiers.

<sup>2</sup>Note that the belief encoding of ground-truth is not related to label smoothing. It maps ground-truth labels from the original class space to a set space without adding noise, thus preserving label "hardness".

### 3.2 Loss function

A Random-Set prediction problem is mathematically similar to the multi-label classification problem, for in both cases the ground truth vector contains several 1s. In the former case, these correspond to sets all containing the true class; in the latter, to all the class labels attached to same data point.

Despite the different semantics, we can thus adopt as loss Binary Cross-Entropy (BCE) (5) with sigmoid activation, to drive the prediction of a belief value for each focal set in the identified budget.

$$\mathcal{L}_{BCE} = - \sum_{i=1}^{b_{size}} \frac{1}{|\mathcal{O}|} \sum_{A \in \mathcal{O}} \left[ Bel_i(A) \log(\hat{Bel}_i(A)) + (1 - Bel_i(A)) \log(1 - \hat{Bel}_i(A)) \right], \quad (5)$$

where  $i$  is the index of the training point within a batch of cardinality  $b_{size}$ ,  $A$  is a focal set of classes in the budget  $\mathcal{O}$ ,  $Bel_i(A)$  is the  $A$ -th component of the vector  $\mathbf{bel}_i$  encoding the ground truth belief values for the  $i$ -th training point, and  $\hat{Bel}_i(A)$  is the corresponding belief value in the predicted vector  $\hat{\mathbf{bel}}_i$  for the same training point. Both  $\mathbf{bel}_i$  and  $\hat{\mathbf{bel}}_i$  are vectors of cardinality  $|\mathcal{O}|$  for all  $i$ .

To ensure that the predicted scores amount to a valid belief function, we incorporate a mass regularization term  $M_r$  in the loss function that encourages non-negativity (1) of the (predicted) mass values  $\hat{m}(A)$ ,  $A \in \mathcal{O}$ , which can be obtained from the predicted belief function  $\hat{\mathbf{bel}}$  via the Moebius inversion formula (2). For it to be valid, the sum of the masses of the predicted belief function must be equal to 1 (1), therefore, we also add a mass sum term  $M_s$ , namely

$$M_s = \max \left( 0, \frac{1}{b_{size}} \sum_{i=1}^{b_{size}} \sum_{A \in \mathcal{O}} \hat{m}_i(A) - 1 \right), \quad M_r = \frac{1}{b_{size}} \sum_{i=1}^{b_{size}} \sum_{A \in \mathcal{O}} \max(0, -\hat{m}_i(A)). \quad (6)$$

All the components  $\mathcal{L}_{BCE}$ ,  $M_r$  and  $M_s$  are computed during batch training. Two hyperparameters,  $\alpha$  and  $\beta$ , control the relative importance of the two mass terms, yielding as the total loss for RS-NN:

$$\mathcal{L}_{RS} = \mathcal{L}_{BCE} + \alpha M_r + \beta M_s. \quad (7)$$

The regularization terms aim to penalize deviations from valid belief functions. When the values of  $\alpha$  and  $\beta$  are too small, the regularization terms may not be sufficient to ensure that predictions are valid belief functions. This occurs because we do not enforce the model to predict valid belief functions during training; rather, we merely encourage it – just like, e.g., training time regularisation in neurosymbolic learning encourages predictions to be commonsense [41]. In such cases,<sup>3</sup> post-training, we fix all negative masses (obtained from predicted belief functions) to zero and introduce a final subset, often referred to as the ‘universal set’ or ‘full set,’ containing all the classes in the powerset, to the final budget  $\mathcal{O}$ . This subset is assigned all the remaining mass, ensuring that the sum of masses across all focal sets in  $\mathcal{O}$  equals 1. This adjustment compensates for the fact that, during clustering, only a few focal sets of classes  $\{A_1, \dots, A_K\}$  from the power set  $\mathbb{P}(\mathcal{C})$  are selected, rather than considering any arbitrary set of classes.

### 3.3 Accuracy and uncertainty estimation

**Pignistic prediction.** The pignistic probability (3) is the central prediction associated with a belief function (seen as a credal set): standard performance metrics such as accuracy can then be calculated after extracting the most likely class according to the pignistic prediction (e.g. in §D.5.3).

**Entropy of the pignistic prediction.** The Shannon entropy of the pignistic prediction  $BetP$  can then be used as a measure of the uncertainty associated with the predictions, in some way analogous to the entropy of a Bayesian mean average prediction:

$$H_{RS} = - \sum_{c \in \mathcal{C}} BetP(c) \log BetP(c). \quad (8)$$

A higher entropy value (8) indicates greater uncertainty in the model’s predictions.

**Size of the credal prediction.** A sensible measure of the epistemic uncertainty attached to a random-set prediction  $\hat{\mathbf{bel}}$  is the size of the corresponding credal set (4). There are several ways of measuring the size of a convex polytope like a credal set [90]. Given the upper and lower bounds to the probability assigned to each class  $c$  by distributions within the predicted credal set  $\hat{C}re$ ,

$$\bar{P}(c) = \max_{P \in \hat{C}re} P(c), \quad \underline{P}(c) = \min_{P \in \hat{C}re} P(c), \quad (9)$$

<sup>3</sup>At any rate, improper belief functions are employed in the literature, e.g. for conditioning [21]

we propose a simple way to measure the size of the credal set as the difference between the lower and upper bounds (9) associated with the most likely class according to the pignistic prediction. For each class  $c$ , not just  $\hat{c}$ , the predicted pignistic estimate  $BetP(c)$  falls within the interval  $[\underline{P}(c), \overline{P}(c)]$ , whose width  $\overline{P}(c) - \underline{P}(c)$  indicates the epistemic uncertainty associated with the prediction (§A.4).

## 4 Experiments

### 4.1 Implementation

**Experiments, datasets and baselines.** **Firstly**, we assess the test accuracy (%) and inference time (ms) on multi-class image classification datasets, including MNIST [67], CIFAR-10 [62], Intel Image [9], CIFAR-100 [61], and ImageNet [24]. Tab. 2 provides a comparison of test accuracies and inference times of RS-NN against state-of-the-art Bayesian methods, R-BNN [59], LB-BNN [51], Ensemble classifier ENN [82] and standard CNN as detailed in Sec. 4.2.

Our **second** set of experiments (Sec. 4.3) concerns out-of-distribution (OoD) detection. Tab. 1 shows our results on OoD detection metrics AUROC (Area Under Receiver Operating Characteristic curve) and AUPRC (Area Under Precision-Recall curve) for RS-NN, LB-BNN, ENN and standard CNN. We provide quantitative assessment on several iD vs OoD datasets: CIFAR-10 vs SVHN [78]/Intel-Image [9], MNIST vs F-MNIST [111]/K-MNIST [16], and ImageNet vs ImageNet-O [49]. We also report the Expected Calibration Error (ECE) for RS-NN, LB-BNN, ENN and standard CNN on datasets CIFAR-10, MNIST and ImageNet (see Tab. 1).

In the **third** set of experiments (Sec. 4.4), we test the uncertainty estimation capabilities of RS-NN using both the entropy of the pignistic prediction and the size of the predicted credal set. Tab. 1 presents the predicted pignistic entropy of RS-NN alongside entropies of LB-BNN, ENN, and CNN on in-distribution (iD) datasets, namely CIFAR-10, MNIST, ImageNet, and out-of-distribution (OoD) datasets CIFAR-10 vs SVHN/Intel Image, MNIST vs F-MNIST/K-MNIST, and ImageNet vs ImageNet-O. Tab. 3 shows credal set widths for RS-NN predictions across the same datasets.

In our **final** set of experiments, we explore the adaptability of RS-NN (Sec. 4.5) to large-scale architectures, employing it on models such as WideResNet-28-10, VGG16, Inception V3, EfficientNetB2 and ViT-Base. Further, to underscore the model’s ability to leverage transfer learning, we conduct training and testing on a pre-trained ResNet50 model initialised with ImageNet weights (Tab. 4).

**Additional experiments** include providing statistical guarantees on RS-NN using non-conformity scores (§A), evaluating the robustness of RS-NN to adversarial attacks (§D.2), noisy and rotated in-distribution samples in Appendix §D.1, how RS-NN circumvents the overconfidence problem in CNNs is given in §D.3. Results showing how credal set width is less correlated with confidence scores than entropy are discussed in in §D.5.1. Ablation studies on  $\alpha$  and  $\beta$  are shown in §D.5.5 and number of non-singleton focal sets ( $K$ ) in §D.5.6. The ablation study demonstrates that the best accuracy is obtained at small values (0 to 1e-2) of  $\alpha$  and  $\beta$ , and  $K = 20$  for CIFAR-10 dataset.

**Baselines and backbones.** All models, including RS-NN, R-BNN, LB-BNN, ENN and standard CNN, are trained on ResNet50 (on 3 NVIDIA A100 80GB GPUs) with a learning rate scheduler initialized at 1e-3 with 0.1 decrease at epochs 80, 120, 160, and 180. Standard data augmentation [63] including random horizontal/vertical shifts with a magnitude of 0.1 and horizontal flips are applied to all models. ResNet50, excluding the top classification layer, serves as the common architecture. ResNet was originally designed for classification on the ImageNet dataset (1000 classes). To accommodate a reduced number of classes in smaller datasets (e.g., CIFAR-10/MNIST with 10 classes, Intel Image with 7 classes, and CIFAR-100 with 100 classes), two additional dense layers (1024 and 512 neurons, ReLU activation) are added to ResNet50. Similar techniques are commonly applied in deep learning to adapt model architectures to different datasets [48, 115]. The output layer of RS-NN on ResNet50 has the same number of units as the number of (selected) focal sets  $|\mathcal{O}|$ , and uses sigmoid activation since the ground truth encoding resembles a multi-label classification problem (see Sec. 3.2). For all other models, the final output layer simply consists of a softmax activation for multi-class classification.

**Training the RS-NN.** We first train a CNN using Adam [58] optimizer on categorical cross-entropy loss over 100 epochs with learning rate scheduler and batch size of 128. The feature vector  $f$  is extracted from the penultimate layer of this trained model for clustering. Alternatively, features can be obtained directly from a pre-trained classifier. In the clustering phase, we use 50 CPU cores (all available), setting a budget  $K$  of 20 focal sets for CIFAR-10/ MNIST/ Intel Image, 200 for CIFAR-100 and 3000 for ImageNet. RS-NN is trained from scratch on ground-truth belief encoding

Table 1: OoD detection performance and uncertainty estimation for models trained on ResNet50 on CIFAR-10 vs SVHN/Intel Image, MNIST vs F-MNIST/K-MNIST and ImageNet vs ImageNet-O. Evaluation metrics include AUROC/AUPRC (OoD); Entropy of predictions (uncertainty) and Expected Calibration Error (ECE).

Dataset	Model	In-distribution (iD)			Out-of-distribution (OoD)						
		Test accuracy (%) ( $\uparrow$ )	Uncertainty measure	In-distribution Entropy ( $\downarrow$ )	ECE ( $\downarrow$ )	SVHN			Intel Image		
						AUROC ( $\uparrow$ )	AUPRC ( $\uparrow$ )	Entropy ( $\uparrow$ )	AUROC ( $\uparrow$ )	AUPRC ( $\uparrow$ )	Entropy ( $\uparrow$ )
CIFAR-10	RS-NN	<b>93.53</b>	Pignistic entropy	<b>0.088 <math>\pm</math> 0.308</b>	<b>0.0484</b>	<b>94.91</b>	<b>93.72</b>	<b>1.132 <math>\pm</math> 0.855</b>	<b>97.39</b>	<b>90.27</b>	<b>1.517 <math>\pm</math> 0.740</b>
	LB-BNN	89.95	Predictive Entropy	0.191 $\pm$ 0.412	0.0585	88.14	81.96	0.828 $\pm$ 0.243	82.21	55.17	0.763 $\pm$ 0.722
	ENN	91.55	Mean Entropy	0.126 $\pm$ 0.323	0.0556	92.76	89.05	0.887 $\pm$ 0.514	85.67	58.09	0.600 $\pm$ 0.578
	CNN	92.08	Softmax Entropy	0.114 $\pm$ 0.304	0.0669	93.11	91.0	0.930 $\pm$ 0.610	87.75	65.54	0.719 $\pm$ 0.673
MNIST	RS-NN	<b>99.71</b>	Pignistic entropy	0.010 $\pm$ 0.111	<b>0.0029</b>	<b>93.89</b>	<b>93.98</b>	<b>0.530 <math>\pm</math> 0.770</b>	<b>96.75</b>	<b>96.58</b>	<b>0.740 <math>\pm</math> 0.917</b>
	LB-BNN	99.58	Predictive Entropy	<b>0.001 <math>\pm</math> 0.085</b>	0.0032	89.65	90.36	0.287 $\pm$ 0.442	95.61	95.65	0.540 $\pm$ 0.621
	ENN	99.07	Mean Entropy	0.022 $\pm$ 0.127	0.0039	81.79	82.92	0.313 $\pm$ 0.464	95.94	95.45	0.703 $\pm$ 0.672
	CNN	98.90	Softmax Entropy	0.023 $\pm$ 0.135	0.0052	83.77	84.14	0.278 $\pm$ 0.426	94.46	93.94	0.616 $\pm$ 0.688
ImageNet	RS-NN	<b>79.92</b>	Pignistic entropy	3.153 $\pm$ 2.549	<b>0.1416</b>	ImageNet-O		Entropy			
	LB-BNN	72.48	Predictive Entropy	2.471 $\pm$ 2.972	0.5812	AUROC	AUPRC				
	ENN	71.82	Mean Entropy	<b>1.395 <math>\pm</math> 1.510</b>	0.5961	<b>60.38</b>	<b>55.16</b>	3.911 $\pm$ 2.318			
	CNN	78.56	Softmax Entropy	6.386 $\pm$ 1.388	0.4004	41.08	30.99	1.383 $\pm$ 0.028			
						54.67	43.73	1.617 $\pm$ 1.597			
						54.28	48.73	<b>6.575 <math>\pm</math> 1.512</b>			

Table 2: Test accuracies (%) and inference time (ms) for uncertainty estimation over 5 consecutive runs across methods and datasets. Average and standard deviation are shown for each experiment.

Datasets	MNIST	CIFAR-10	Intel Image	CIFAR-100	ImageNet (Top-1)	ImageNet (Top-5)	Inference time (ms)
CNN	98.90 $\pm$ 0.04	92.08 $\pm$ 0.42	90.89 $\pm$ 0.10	65.50 $\pm$ 0.08	78.56	94.34	<b>1.91 <math>\pm</math> 0.03</b>
R-BNN [60]	90.32 $\pm$ 0.14	75.21 $\pm$ 0.13	82.12 $\pm$ 0.08	50.45 $\pm$ 0.02	-	-	62.17 $\pm$ 0.76
LB-BNN [51]	99.58 $\pm$ 0.04	89.95 $\pm$ 0.81	90.49 $\pm$ 0.42	59.89 $\pm$ 1.96	72.48	90.85	7.11 $\pm$ 0.89
ENN [82]	99.07 $\pm$ 0.11	91.55 $\pm$ 0.60	91.49 $\pm$ 0.19	68.02 $\pm$ 0.26	71.82	89.48	3.10 $\pm$ 0.03
<b>RS-NN</b>	<b>99.71 <math>\pm</math> 0.03</b>	<b>93.53 <math>\pm</math> 0.09</b>	<b>94.22 <math>\pm</math> 0.03</b>	<b>71.61 <math>\pm</math> 0.07</b>	<b>79.92</b>	<b>94.47</b>	<b>1.91 <math>\pm</math> 0.02</b>

of sets using the  $\mathcal{L}_{RS}$  loss function (7) over 200 epochs, with a batch size ( $b_{size}$ ) of 128. The data is split into 40000:10000:10000 samples for training, testing, and validation respectively for CIFAR-10 and CIFAR-100, 50000:10000:10000 samples for MNIST, 13934:3000:100 samples for Intel Image, 1172498:50000:108669 for ImageNet. For all OoD datasets, we use 10,000 testing samples except for Intel Image (CIFAR-10 vs Intel Image), we use 3000 samples. All datasets are resized to  $224 \times 224$ .

## 4.2 Comparison with the state-of-the-art on accuracy

Tab. 2 shows RS-NN outperform state-of-the-art Bayesian (R-BNN, LB-BNN) and Ensemble (ENN) methods in terms of test accuracy (%) across all datasets. On ImageNet, RS-NN’s accuracy is remarkably close to CNN (standard ResNet50), highlighting its efficacy on large and complex datasets. It is important to note that the comparison with standard CNNs is not based on their role as uncertainty methods, but as benchmarks, underscoring RS-NN’s effectiveness in achieving high accuracy compared to other uncertainty baselines. Test accuracy for RS-NN is calculated by determining the class with the highest pignistic probability for each prediction and comparing it with the true class. As RS-NN leverages a random set framework which does not require prior assumptions and is more data driven, it can better adapt and capture the inherent complexity of the data, contributing to its superior performance in test accuracy across various datasets (Tab. 2). The pignistic predictions derived from the predicted belief functions appear more reliable and accurate than standard predicted probabilities of a CNN. R-BNN results for ImageNet are not reported in Tab. 2 as evaluating it on large-scale datasets is impractical due to its complexity. Experiments on inference time (ms) per sample over 5 runs (a single forward propagation) on CIFAR-10 dataset demonstrates the fastest inference time (ms) for RS-NN among all models (Tab. 2).

## 4.3 Out-of-distribution (OoD) detection

We evaluate out-of-distribution (OoD) detection (Tab. 1) against baselines using AUROC and AUPRC scores. OoD detection identifies data points deviating from the in-distribution (iD) training data by measuring true and false positive rates (AUROC) and precision and recall trade-offs (AUPRC), providing insights into the model’s performance at varying confidence levels (detailed in §C.3).

RS-NN greatly outperforms Bayesian, Ensemble and standard CNN models in OoD detection (Tab. 1), with significantly higher AUROC and AUPRC scores for all iD vs OoD datasets, especially on CIFAR-10 vs SVHN/Intel Image. This demonstrates its effectiveness in identifying data points deviating from training data. In real-world scenarios, encountering OoD instances is inevitable. Reliable OoD detection is crucial for safety-critical applications to prevent erroneous critical decisions on unfamiliar or anomalous data. Recognising unfamiliar data signals the model about situations beyond its training, allowing it to acknowledge its own limitations and enhance its awareness of ignorance, achieved effectively by RS-NN. Tab. 1 also reports the Expected Calibration Error (ECE) (detailed in §C.2).



Table 3: Credal set width for RS-NN on iD vs OoD datasets: CIFAR10 vs SVHN/Intel Image, MNIST vs F-MNIST/K-MNIST and ImageNet vs ImageNet-O.

In-distribution (iD)		Out-of-distribution (OoD)			
CIFAR10	0.007 ± 0.044	SVHN	0.260 ± 0.322	Intel Image	0.587 ± 0.367
MNIST	0.001 ± 0.013	F-MNIST	0.070 ± 0.167	K-MNIST	0.103 ± 0.200
ImageNet	0.238 ± 0.266	ImageNet-O	0.272 ± 0.275		

Table 4: Adaptability to large-scale model architectures with test accuracy (%) and parameters (in million) reported on CIFAR10.

	Model	Pre-trained R50	WRN-28-10	VGG16	IncepV3	ENetB2	ViT-Base
Test acc. (%)	RS-NN	<b>94.42</b>	<b>93.58</b>	<b>87.87</b>	<b>78.24</b>	<b>92.10</b>	86.75
	CNN	94.38	92.79	84.14	76.89	90.02	<b>87.21</b>
Params (M)	RS-NN	2.69	37.0	15.12	31.22	7.72	9.53
	CNN	2.62	36.7	15.11	31.21	7.71	9.52

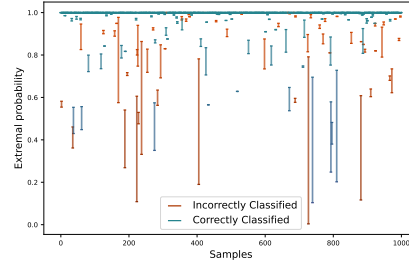


Figure 6: Width of credal predictions for 1,000 CIFAR-10 test samples (correctly classified, blue; incorrectly classified, orange).

A low ECE indicates that the model’s confidence scores align closely with the actual likelihood of events. RS-NN exhibits the lowest ECE indicating well-calibrated probabilistic predictions.

#### 4.4 Uncertainty estimation

**Entropy.** Tab. 1 shows the mean and variance of the entropy distributions for both iD and OoD datasets. Lower entropy values for iD datasets indicate a confident prediction as the model is trained on familiar data, while higher entropy for OoD datasets reflects the model’s uncertainty with unseen data. RS-NN exhibits both low entropy for iD datasets and high entropy for OoD ones. The percentage mean iD/OoD shift in entropy is most pronounced in RS-NN, especially evident in ImageNet, where CNN exhibits high entropy for iD and OoD datasets. RS-NN maintains a desirable iD vs OoD entropy ratio. This ideal behavior, along with superior OoD detection (Sec. 4.3), is a good indication that RS-NN is better at estimating uncertainty induced by domain shift (see §D.5.2).

**Credal set width.** Fig. 6 displays the estimated credal set width, the difference between the lower and upper probability bounds in (9), for correctly and incorrectly classified classifications of 1000 CIFAR-10 test samples. Incorrect predictions (orange) correlate with larger credal set widths, indicating higher epistemic uncertainty, and are dispersed in the middle of the plot. Correct predictions (blue) concentrate at the top, exhibiting smaller credal intervals as expected. Some instances of correct classification still display a sizable credal set width, signifying elevated uncertainty and low confidence. Tab. 3 reports the credal set widths of RS-NN predictions for iD vs OoD datasets. Larger intervals can be observed for OoD datasets. Note that credal set width is not directly comparable to the entropy or variance of other models, as such metrics have distinct semantics.

#### 4.5 Adaptability to large-scale architectures

Tab. 4 shows the adaptability of RS-NN to larger model architectures and its ability to leverage transfer learning. RS-NN demonstrates higher accuracy compared to standard CNNs across various large-scale model architectures, including WideResNet28-10 (WRN-28-10), VGG16, InceptionV3 (IncV3), EfficientNetB2 (ENetB2), and to Vision Transformer (ViT-Base), showcasing its versatility and ease in adopting different architectures and the generality of the random-set concept. Notably, using a pre-trained ResNet50 (Pre-trained R50) model with ImageNet weights, RS-NN achieves higher accuracy on CIFAR-10 compared to using only the architecture (no pre-trained weights).

#### 4.6 Limitations

The budgeting step can be time consuming but, for a given dataset, it is a one-time procedure prior to training. For large datasets, t-SNE and GMM can be applied to representative samples rather than the entire dataset, as the purpose is merely to identify the most relevant sets, reducing computational demands. To further optimise the method, instead of t-SNE, budgeting can utilize various methods such as autoencoders [40, 46] or PCA [1] for dimensionality reduction. However, despite the initial time investment, the efficiency gained from having a budget applicable to any training scenario is substantial. Another limitation is manually setting the number of focal elements  $K$ ; a dynamic strategy adjusting  $K$  based on overlap would enhance flexibility and effectiveness. The budgeting procedure can also be adapted to work with multiple sources of data or a stream of data (§D.4). Alternative methods such as using sparse mass functions [54, 15], could provide a quantitative basis for determining the subsets  $A_K$  to consider.

## 5 Conclusion

This paper proposes a novel *Random-Set Neural Network (RS-NN)* for uncertainty estimation in classification using belief functions and random sets. Random-set representation is a foundational method that acts as a versatile wrapper and extends beyond CNNs to any model architecture and classification task (e.g, text). To our knowledge, this concept, along with budgeting for optimal selection of sets, is unprecedented. RS-NN outperforms state-of-the-art uncertainty estimation models and the standard CNN in performance and out-of-distribution OoD tests, and scales seamlessly to large-scale architectures and datasets. Given such results, our approach exhibits significant potential impact for safety-critical applications such as medical diagnostics and autonomous driving, where uncertainty estimation and OoD detection is crucial. In this paper, we discuss target-level representation of RS-NNs. Future work involves parameter-level representation of RS-NN and the extension of this concept from classification to detection tasks.

## Acknowledgement

This work has received funding from the European Union’s Horizon 2020 research and innovation program under grant agreement No. 964505 (E-pi).

## References

- [1] Hervé Abdi and Lynne J Williams. Principal component analysis. *Wiley interdisciplinary reviews: computational statistics*, 2(4):433–459, 2010.
- [2] Charu C Aggarwal, Xiangnan Kong, Quanquan Gu, Jiawei Han, and S Yu Philip. Active learning: A survey. In *Data Classification: Algorithms and Applications*, pages 571–605. CRC Press, 2014.
- [3] Anastasios N Angelopoulos and Stephen Bates. A gentle introduction to conformal prediction and distribution-free uncertainty quantification. *arXiv preprint arXiv:2107.07511*, 2021.
- [4] Anastasios N Angelopoulos and Stephen Bates. A gentle introduction to conformal prediction and distribution-free uncertainty quantification. *arXiv preprint arXiv:2107.07511*, 2021.
- [5] Alessandro Antonucci and Giorgio Corani. The multilabel Naive Credal Classifier. *International Journal of Approximate Reasoning*, 83:320–336, 2017.
- [6] Alessandro Antonucci and Fabio Cuzzolin. Credal sets approximation by lower probabilities: application to credal networks. In *Computational Intelligence for Knowledge-Based Systems Design: 13th International Conference on Information Processing and Management of Uncertainty, IPMU 2010, Dortmund, Germany, June 28-July 2, 2010. Proceedings 13*, pages 716–725. Springer, 2010.
- [7] Alessandro Antonucci and Fabio Cuzzolin. Credal sets approximation by lower probabilities: Application to credal networks. In Eyke Hüllermeier, Rudolf Kruse, and Frank Hoffmann, editors, *Computational Intelligence for Knowledge-Based Systems Design*, volume 6178 of *Lecture Notes in Computer Science*, pages 716–725. Springer, Berlin Heidelberg, 2010.
- [8] Vineeth Balasubramanian, Shen-Shyang Ho, and Vladimir Vovk. *Conformal prediction for reliable machine learning: theory, adaptations and applications*. Newnes, 2014.
- [9] Puneet Bansal. Intel image classification. Available on <https://www.kaggle.com/puneet6060/intel-image-classification>, Online, 2019.
- [10] Daniel Barbara and Ping Chen. Tracking clusters in evolving data sets. In *FLAIRS*, pages 239–243, 2001.
- [11] Jonathan Baron. Second-order probabilities and belief functions. *Theory and Decision*, 23:25–36, 1987.
- [12] WL Buntine and AS Weigend. Bayesian back-propagation. Technical Report FIA-91-22, 1991.
- [13] Thomas Burger, Oya Aran, and Alice Caplier. Modeling hesitation and conflict: a belief-based approach for multi-class problems. In *2006 5th International Conference on Machine Learning and Applications (ICMLA’06)*, pages 95–100. IEEE, 2006.

- [14] Alain Chateaufneuf and Jean-Yves Jaffray. Some characterizations of lower probabilities and other monotone capacities through the use of Möbius inversion. *Mathematical Social Sciences*, 17(3):263–283, 1989.
- [15] Phil Chen, Mikhail Itkina, Ransalu Senanayake, and Mykel J Kochenderfer. Evidential softmax for sparse multimodal distributions in deep Generative models. *Advances in Neural Information Processing Systems*, 34:11565–11576, 2021.
- [16] Tarin Clanuwat, Mikel Bober-Irizar, Asanobu Kitamoto, Alex Lamb, Kazuaki Yamamoto, and David Ha. Deep learning for classical Japanese literature. *arXiv preprint arXiv:1812.01718*, 2018.
- [17] Giorgio Corani and Marco Zaffalon. Learning reliable classifiers from small or incomplete data sets: The naive credal classifier 2. *Journal of Machine Learning Research*, 9:581–621, 04 2008.
- [18] Fabio Cuzzolin. On the credal structure of consistent probabilities. In *European Workshop on Logistics in Artificial Intelligence*, pages 126–139. Springer, 2008.
- [19] Fabio Cuzzolin. Credal semantics of Bayesian transformations in terms of probability intervals. *IEEE Transactions on Systems, Man, and Cybernetics, Part B: Cybernetics*, 40(2):421–432, 2010.
- [20] Fabio Cuzzolin. Visions of a generalized probability theory. *arXiv preprint arXiv:1810.10341*, 2018.
- [21] Fabio Cuzzolin. *The Geometry of Uncertainty: The Geometry of Imprecise Probabilities*. Artificial Intelligence: Foundations, Theory, and Algorithms. Springer International Publishing, 2020.
- [22] Erik Daxberger, Agustinus Kristiadi, Alexander Immer, Runa Eschenhagen, Matthias Bauer, and Philipp Hennig. Laplace Redux - Effortless Bayesian Deep Learning. In M. Ranzato, A. Beygelzimer, Y. Dauphin, P.S. Liang, and J. Wortman Vaughan, editors, *Advances in Neural Information Processing Systems*, volume 34, pages 20089–20103. Curran Associates, Inc., 2021.
- [23] Arthur P Dempster. Upper and lower probabilities induced by a multivalued mapping. In *Classic works of the Dempster-Shafer theory of belief functions*, pages 57–72. Springer, 2008.
- [24] Jia Deng, Wei Dong, Richard Socher, Li-Jia Li, Kai Li, and Li Fei-Fei. Imagenet: A large-scale hierarchical image database. In *2009 IEEE Conference on Computer Vision and Pattern Recognition*, pages 248–255. Ieee, 2009.
- [25] Thierry Denœux. A neural network classifier based on Dempster-Shafer theory. *IEEE Transactions on Systems, Man, and Cybernetics - Part A: Systems and Humans*, 30(2):131–150, 2000.
- [26] Thierry Denœux. Constructing belief functions from sample data using multinomial confidence regions. *International Journal of Approximate Reasoning*, 42(3):228–252, 2006.
- [27] Thierry Denœux. A k-nearest neighbor classification rule based on Dempster-Shafer theory. In Roland R. Yager and Liping Liu, editors, *Classic Works of the Dempster-Shafer Theory of Belief Functions*, volume 219 of *Studies in Fuzziness and Soft Computing*, pages 737–760. Springer, 2008.
- [28] Thierry Denœux. An evidential neural network model for regression based on random fuzzy numbers. In *International Conference on Belief Functions*, pages 57–66. Springer, 2022.
- [29] Javier Diaz-Rozo, Concha Bielza, and Pedro Larrañaga. Clustering of data streams with dynamic gaussian mixture models: An iot application in industrial processes. *IEEE Internet of Things Journal*, 5(5):3533–3547, 2018.
- [30] Didier Dubois and Henri Prade. Consonant approximations of belief functions. *International Journal of Approximate Reasoning*, 4:419–449, 1990.
- [31] Zied Elouedi, Khaled Mellouli, and Philippe Smets. Decision trees using the belief function theory. In *Proceedings of the Eighth International Conference on Information Processing and Management of Uncertainty in Knowledge-based Systems (IPMU 2000)*, volume 1, pages 141–148, Madrid, 2000.

- [32] Zied Elouedi<sup>1</sup>, Khaled Mellouli<sup>1</sup>, and Philippe Smets. Classification with belief decision trees. In *International Conference on Artificial Intelligence: Methodology, Systems, and Applications*, pages 80–90. Springer, 2000.
- [33] Rebecca Fay, Friedhelm Schwenker, Christian Thiel, and Günther Palm. Hierarchical neural networks utilising dempster-shafer evidence theory. In Friedhelm Schwenker and Simone Marinai, editors, *Artificial Neural Networks in Pattern Recognition*, pages 198–209, Berlin, Heidelberg, 2006. Springer Berlin Heidelberg.
- [34] Vincent Fortuin. Priors in Bayesian Deep Learning: A Review. *International Statistical Review*, 90, 05 2022.
- [35] David Freedman. Wald lecture: On the Bernstein-von Mises theorem with infinite-dimensional parameters. *The Annals of Statistics*, 27(4):1119–1141, 1999.
- [36] Zhun ga Liu, Jean Dezert, Grégoire Mercier, and Quan Pan. Belief C-means: An extension of fuzzy C-means algorithm in belief functions framework. *Pattern Recognition Letters*, 33(3):291–300, 2012.
- [37] Yarin Gal and Zoubin Ghahramani. Bayesian convolutional neural networks with Bernoulli approximate variational inference. *arXiv preprint arXiv:1506.02158*, 2015.
- [38] Yarin Gal and Zoubin Ghahramani. Dropout as a Bayesian approximation: Representing model uncertainty in deep learning. In *International Conference on Machine Learning*, pages 1050–1059. PMLR, 2016.
- [39] Yonatan Geifman and Ran El-Yaniv. Selective classification for deep neural networks. *arXiv:1705.08500*, 2017.
- [40] Kamran Ghasedi Dizaji, Amirhossein Herandi, Cheng Deng, Weidong Cai, and Heng Huang. Deep clustering via joint convolutional autoencoder embedding and relative entropy minimization. In *Proceedings of the IEEE international conference on computer vision*, pages 5736–5745, 2017.
- [41] Eleonora Giunchiglia, Mihaela Cătălina Stoian, Salman Khan, Fabio Cuzzolin, and Thomas Lukasiewicz. Road-r: The autonomous driving dataset with logical requirements. *Machine Learning*, 112(9):3261–3291, 2023.
- [42] Wenjuan Gong and Fabio Cuzzolin. A belief-theoretical approach to example-based pose estimation. *IEEE Transactions on Fuzzy Systems*, 26(2):598–611, 2018.
- [43] Ian J Goodfellow, Jonathon Shlens, and Christian Szegedy. Explaining and harnessing adversarial examples. *arXiv preprint arXiv:1412.6572*, 2014.
- [44] Andreas Graefe, Helmut Küchenhoff, Veronika Stierle, and Bernhard Riedl. Limitations of ensemble Bayesian model averaging for forecasting social science problems. *International Journal of Forecasting*, 31(3):943–951, 2015.
- [45] Chuan Guo, Geoff Pleiss, Yu Sun, and Kilian Q Weinberger. On calibration of modern neural networks. In *International conference on machine learning*, pages 1321–1330. PMLR, 2017.
- [46] Xifeng Guo, Xinwang Liu, En Zhu, and Jianping Yin. Deep clustering with convolutional autoencoders. In *Neural Information Processing: 24th International Conference, ICONIP 2017, Guangzhou, China, November 14-18, 2017, Proceedings, Part II 24*, pages 373–382. Springer, 2017.
- [47] Joseph Y. Halpern. *Reasoning About Uncertainty*. MIT Press, 2017.
- [48] Kaiming He, Xiangyu Zhang, Shaoqing Ren, and Jian Sun. Deep residual learning for image recognition. In *Proceedings of the IEEE Conference on Computer Vision and Pattern Recognition (CVPR)*, June 2016.
- [49] Dan Hendrycks, Kevin Zhao, Steven Basart, Jacob Steinhardt, and Dawn Song. Natural adversarial examples. In *Proceedings of the IEEE/CVF Conference on Computer Vision and Pattern Recognition*, pages 15262–15271, 2021.
- [50] Max Hinne, Quentin F Gronau, Don van den Bergh, and Eric-Jan Wagenmakers. A conceptual introduction to Bayesian model averaging. *Advances in Methods and Practices in Psychological Science*, 3(2):200–215, 2020.

- [51] Marius Hobbhahn, Agustinus Kristiadi, and Philipp Hennig. Fast predictive uncertainty for classification with Bayesian deep networks. In *Uncertainty in Artificial Intelligence*, pages 822–832. PMLR, 2022.
- [52] Marius Hobbhahn, Agustinus Kristiadi, and Philipp Hennig. Fast predictive uncertainty for classification with Bayesian deep networks. In James Cussens and Kun Zhang, editors, *Proceedings of the Thirty-Eighth Conference on Uncertainty in Artificial Intelligence*, volume 180 of *Proceedings of Machine Learning Research*, pages 822–832. PMLR, 01–05 Aug 2022.
- [53] Eyke Hüllermeier and Willem Waegeman. Aleatoric and epistemic uncertainty in machine learning: An introduction to concepts and methods. *Machine Learning*, 110(3):457–506, 2021.
- [54] Masha Itkina, Boris Ivanovic, Ransalu Senanayake, Mykel J Kochenderfer, and Marco Pavone. Evidential sparsification of multimodal latent spaces in conditional variational autoencoders. *Advances in Neural Information Processing Systems*, 33:10235–10246, 2020.
- [55] Laurent Valentin Jospin, Hamid Laga, Farid Boussaid, Wray Buntine, and Mohammed Benamoun. Hands-on bayesian neural networks—a tutorial for deep learning users. *IEEE Computational Intelligence Magazine*, 17(2):29–48, 2022.
- [56] Alex Kendall and Yarin Gal. What uncertainties do we need in Bayesian deep learning for computer vision? *arXiv:1703.04977*, 2017.
- [57] David G. Kendall. Foundations of a theory of random sets. In E. F. Harding and D. G. Kendall, editors, *Stochastic Geometry*, pages 322–376. Wiley, London, 1974.
- [58] Diederik P Kingma and Jimmy Ba. Adam: A method for stochastic optimization. *arXiv preprint arXiv:1412.6980*, 2014.
- [59] Diederik P Kingma and Max Welling. Auto-encoding Variational Bayes. *arXiv preprint arXiv:1312.6114*, 2013.
- [60] Durk P Kingma, Tim Salimans, and Max Welling. Variational dropout and the local Reparameterization trick. *Advances in Neural Information Processing Systems*, 28, 2015.
- [61] Alex Krizhevsky. Learning multiple layers of features from tiny images. *University of Toronto*, 2012.
- [62] Alex Krizhevsky, Vinod Nair, and Geoffrey Hinton. CIFAR-10 (Canadian Institute For Advanced Research). Technical report, CIFAR, 2009.
- [63] Alex Krizhevsky, Ilya Sutskever, and Geoffrey E Hinton. Imagenet classification with deep convolutional neural networks. In F. Pereira, C.J. Burges, L. Bottou, and K.Q. Weinberger, editors, *Advances in Neural Information Processing Systems*, volume 25. Curran Associates, Inc., 2012.
- [64] Brian Kulis and Michael I Jordan. Revisiting k-means: New algorithms via bayesian nonparametrics. *arXiv preprint arXiv:1111.0352*, 2011.
- [65] Hicham Laanaya, Arnaud Martin, Driss Aboutajdine, and Ali Khenchaf. Support vector regression of membership functions and belief functions – Application for pattern recognition. *Information Fusion*, 11(4):338–350, 2010.
- [66] Balaji Lakshminarayanan, Alexander Pritzel, and Charles Blundell. Simple and Scalable Predictive Uncertainty Estimation using Deep Ensembles. *Advances in Neural Information Processing Systems*, 30, 2017.
- [67] Yann LeCun and Corinna Cortes. The MNIST database of handwritten digits. In *Proceedings of the IEEE Conference on Computer Vision and Pattern Recognition (CVPR)*, pages 1–9, 2005.
- [68] Isaac Levi. *The enterprise of knowledge: An essay on knowledge, credal probability, and chance*. The MIT Press, Cambridge, Massachusetts, 1980.
- [69] David J. C. MacKay. A Practical Bayesian Framework for Backpropagation Networks. *Neural Computation*, 4(3):448–472, 05 1992.
- [70] Shireen Kudukkil Manchingal and Fabio Cuzzolin. Epistemic deep learning. *arXiv preprint arXiv:2206.07609*, 2022.
- [71] Ryan Martin and Chuanhai Liu. Inferential models: A framework for prior-free posterior probabilistic inference. *Journal of the American Statistical Association*, 108(501):301–313, 2013.

- [72] Ryan Martin and Chuanhai Liu. *Inferential models: reasoning with uncertainty*. CRC Press, 2015.
- [73] Georges Matheron. *Random sets and integral geometry*. Wiley Series in Probability and Mathematical Statistics, New York, 1975.
- [74] Ilya Molchanov. Random sets and random functions. *Theory of Random Sets*, pages 451–552, 2017.
- [75] Ilya S Molchanov. *Theory of random sets*, volume 19. Springer, 2005.
- [76] Thomas Mortier, Marek Wydmuch, Krzysztof Dembczyński, Eyke Hüllermeier, and Willem Waegeman. Efficient set-valued prediction in multi-class classification. *Data Mining and Knowledge Discovery*, 35(4):1435–1469, 2021.
- [77] Radford M Neal. *Bayesian learning for neural networks*, volume 118. Springer Science & Business Media, 2012.
- [78] Yuval Netzer, Tao Wang, Adam Coates, Alessandro Bissacco, Baolin Wu, Andrew Y Ng, et al. Reading digits in natural images with unsupervised feature learning. In *NIPS workshop on deep learning and unsupervised feature learning*, page 7. Granada, Spain, 2011.
- [79] Hung T. Nguyen. On random sets and belief functions. *Journal of Mathematical Analysis and Applications*, 65:531–542, 1978.
- [80] Vu-Linh Nguyen, Sébastien Destercke, Marie-Hélène Masson, and Eyke Hüllermeier. Reliable multi-class classification based on pairwise epistemic and aleatoric uncertainty. In *Proceedings of the Twenty-Seventh International Joint Conference on Artificial Intelligence, IJCAI-18*, pages 5089–5095. International Joint Conferences on Artificial Intelligence Organization, 7 2018.
- [81] Ilia Nourtdinov, Tom Melliush, and Volodya Vovk. Ridge regression confidence machine. In *Proceedings of the Eighteenth International Conference on Machine Learning*, pages 385–392. Morgan Kaufmann, 2001.
- [82] Ian Osband, Zheng Wen, Seyed Mohammad Asghari, Vikranth Dwaracherla, Morteza Ibrahimi, Xiuyuan Lu, and Benjamin Van Roy. Epistemic neural networks. *Advances in Neural Information Processing Systems*, 36, 2024.
- [83] Harris Papadopoulos, Alex Gammerman, and Volodya Vovk. Normalized nonconformity measures for regression conformal prediction. In *Proceedings of the 26th IASTED International Conference on Artificial Intelligence and Applications, AIA '08*, page 64–69, USA, 2008. ACTA Press.
- [84] Harris Papadopoulos, Kostas Proedrou, Volodya Vovk, and Alex Gammerman. Inductive confidence machines for regression. In Tapio Elomaa, Heikki Mannila, and Hannu Toivonen, editors, *Machine Learning: ECML 2002*, pages 345–356, Berlin, Heidelberg, 2002. Springer Berlin Heidelberg.
- [85] Harris Papadopoulos, Vladimir Vovk, and Alexander Gammerman. Qualified prediction for large data sets in the case of pattern recognition. In *ICMLA*, pages 159–163, 2002.
- [86] Nicolas Papernot, Patrick McDaniel, Somesh Jha, Matt Fredrikson, Z Berkay Celik, and Ananthram Swami. The limitations of deep learning in adversarial settings. In *2016 IEEE European Symposium on Security and Privacy (EuroS&P)*, pages 372–387, 2016.
- [87] Kostas Proedrou, Ilia Nourtdinov, Volodya Vovk, and Alex Gammerman. Transductive confidence machines for pattern recognition. In Tapio Elomaa, Heikki Mannila, and Hannu Toivonen, editors, *Machine Learning: ECML 2002*, pages 381–390, Berlin, Heidelberg, 2002. Springer.
- [88] Galina Rogova. Combining the results of several neural network classifiers. *Classic Works of the Dempster-Shafer Theory of Belief Functions*, pages 683–692, 2008.
- [89] Tim GJ Rudner, Zonghao Chen, Yee Whye Teh, and Yarin Gal. Tractable function-space variational inference in Bayesian neural networks. *Advances in Neural Information Processing Systems*, 35:22686–22698, 2022.
- [90] Yusuf Sale, Michele Caprio, and Eyke Hüllermeier. Is the volume of a credal set a good measure for epistemic uncertainty? In *Uncertainty in Artificial Intelligence*, pages 1795–1804. PMLR, 2023.

- [91] Craig Saunders, Alexander Gammerman, and Volodya Vovk. Transduction with confidence and credibility. In *Proceedings of the Sixteenth International Joint Conference on Artificial Intelligence, IJCAI '99*, page 722–726, San Francisco, CA, USA, 1999. Morgan Kaufmann Publishers Inc.
- [92] Murat Sensoy, Lance Kaplan, and Melih Kandemir. Evidential deep learning to quantify classification uncertainty. In *Proceedings of the 32nd International Conference on Neural Information Processing Systems, NIPS'18*, page 3183–3193, Red Hook, NY, USA, 2018. Curran Associates Inc.
- [93] Glenn Shafer. *A mathematical theory of evidence*, volume 42. Princeton university press, 1976.
- [94] Glenn Shafer and Vladimir Vovk. A tutorial on Conformal Prediction. *Journal of Machine Learning Research*, 9(3), 2008.
- [95] Philippe Smets. Decision making in the TBM: the necessity of the pignistic transformation. *International Journal of Approximate Reasoning*, 38(2):133–147, 2005.
- [96] Philippe Smets. Decision making in the TBM: the necessity of the pignistic transformation. *International Journal of Approximate Reasoning*, 38(2):133–147, February 2005.
- [97] Philippe Smets. Bayes' theorem generalized for belief functions. In *Proceedings of the 7th European Conference on Artificial Intelligence (ECAI-86)*, volume 2, pages 169–171, July 1986.
- [98] Philippe Smets and Robert Kennes. The transferable belief model. *Artificial intelligence*, 66(2):191–234, 1994.
- [99] Vincent Spruyt. How to draw a covariance error ellipse. 2014. *Computer Vision for Dummies*. [Available Online-<http://www.visiondummy.com/2014/04/drawerror-ellipse-representing-covariance-matrix/>], 2013.
- [100] Zheng Tong, Philippe Xu, and Thierry Denooux. An evidential classifier based on Dempster-Shafer theory and deep learning. *Neurocomputing*, 450:275–293, 2021.
- [101] Salsabil Trabelsi, Zied Elouedi, and Pawan Lingras. Classification systems based on rough sets under the belief function framework. *Int. J. Approx. Reason.*, 52:1409–1432, 2011.
- [102] Ba-Hien Tran, Simone Rossi, Dimitrios Milios, and Maurizio Filippone. All you need is a good functional prior for Bayesian deep learning. *arXiv preprint arXiv:2011.12829*, 2020.
- [103] Laurens van der Maaten and Geoffrey Hinton. Visualizing data using t-sne. *Journal of Machine Learning Research*, 9(86):2579–2605, 2008.
- [104] Patrick Vannoorenberghe and Philippe Smets. Partially supervised learning by a credal em approach. In Lluís Godo, editor, *Symbolic and Quantitative Approaches to Reasoning with Uncertainty*, pages 956–967, Berlin, Heidelberg, 2005. Springer Berlin Heidelberg.
- [105] Vladimir Vovk. Cross-conformal predictors. *Annals of Mathematics and Artificial Intelligence*, 74, 08 2012.
- [106] Vladimir Vovk, Alexander Gammerman, and Glenn Shafer. *Algorithmic learning in a random world*. Springer Science & Business Media, 2005.
- [107] Vladimir Vovk and Ivan Petej. Venn-abers predictors. *arXiv preprint arXiv:1211.0025*, 2012.
- [108] Vladimir Vovk, Glenn Shafer, and Ilia Nouredinov. Self-calibrating probability forecasting. In S. Thrun, L. Saul, and B. Schölkopf, editors, *Advances in Neural Information Processing Systems*, volume 16. MIT Press, 2003.
- [109] Peter Walley. *Statistical Reasoning with Imprecise Probabilities*. Chapman and Hall, New York, 1991.
- [110] Anton Wallner. Maximal number of vertices of polytopes defined by f-probabilities. In Fabio Gagliardi Cozman, R. Nau, and Teddy Seidenfeld, editors, *Proceedings of the Fourth International Symposium on Imprecise Probabilities and Their Applications (ISIPTA 2005)*, pages 388–395, 2005.
- [111] Han Xiao, Kashif Rasul, and Roland Vollgraf. Fashion-MNIST: a novel image dataset for benchmarking machine learning algorithms. *arXiv preprint arXiv:1708.07747*, 2017.

- [112] L. Xu, A. Krzyzak, and C.Y. Suen. Methods of combining multiple classifiers and their applications to handwriting recognition. *IEEE Transactions on Systems, Man, and Cybernetics*, 22(3):418–435, 1992.
- [113] Marco Zaffalon. The Naive Credal Classifier. *Journal of Statistical Planning and Inference - J STATIST PLAN INFER*, 105:5–21, 06 2002.
- [114] Marco Zaffalon and Enrico Fagiuoli. Tree-based credal networks for classification. *Reliable computing*, 9(6):487–509, 2003.
- [115] Sergey Zagoruyko and Nikos Komodakis. Wide residual networks. *arXiv preprint arXiv:1605.07146*, 2016.



## A Further discussion

### A.1 Rationale and applicability

This paper aims to establish a foundational approach for integrating belief functions into standard deep learning models, specifically CNNs. We chose to closely adhere to a standard CNN framework to ensure the model’s applicability to large-scale, real-world datasets—a capability often lacking in other uncertainty models. As a result, we achieve performance comparable to that of a standard CNN while providing improved and reliable uncertainty estimation.

However, the proposed method can be thought of as a generalisation of traditional classification. There is nothing limiting it to CNNs. In fact, Tab. 4 shows that it can be easily adapted to work with a wide range of network architectures, including Vision Transformers (ViTs). Similarly, it can also work with simple Multi-Layer Perceptrons (MLPs).

### A.2 Statistical guarantees

To complement the extensive discussion in the main paper, we provide here an in-depth discussion on the statistical guarantees underlying RS-NN and the rationale behind our choices for ground-truth representation  $\text{bel}$ , loss function and training, under how RS-NN learns sets of outcomes.

Unlike, e.g., conformal learning, our RS-NN approach does not, in its current state, provide statistical guarantees such as the coverage of the prediction intervals. However, we can see at least three ways in which this could be done.

Firstly, RS-NN can be employed as the ‘underlying model’ in an inductive conformal learning framework ([https://cml.rhul.ac.uk/copa2017/presentations/CP\\_Tutorial\\_2017.pdf](https://cml.rhul.ac.uk/copa2017/presentations/CP_Tutorial_2017.pdf)), which builds an empirical cumulative distribution of the ‘non-conformity’ scores of a set of calibration samples, and at test time outputs the set of labels whose empirical CDF is above a desired significance level  $\epsilon$  (e.g., 95%).

Given a test input  $x$  and the associated predictive belief function  $\hat{B}el(c|x)$  (the output of RS-NN), we could, for instance, set as non-conformity score

$$s(x, c) \doteq 1 - \hat{P}l(c|x) = \hat{B}el(\mathcal{C} \setminus \{c\}|x) \quad (10)$$

(i.e., a label  $c$  is ‘non-conformal’ if its predicted *plausibility*, which is defined as  $Pl(A) = 1 - Bel(\Theta \setminus A)$  and has the semantic of an upper probability bound [93], is low), and compute predictive regions in the usual way:

$$\Gamma(x) = \{c \in \mathcal{C} : p^c > \epsilon\},$$

where

$$p^c = \frac{|(x_j, c_j) : s(x_j, c_j) > s(x, c)|}{q + 1} + u \cdot \frac{|(x_j, c_j) : s(x_j, c_j) = s(x, c)|}{q + 1},$$

$(x_j, c_j)$  is the  $j$ -th calibration point,  $q$  is the number of calibration points, and  $u \sim \mathcal{U}(0, 1)$  (the uniform distribution on the interval  $(0, 1)$ ).

**Experiments on conformal guarantees.** We conducted experiments on CIFAR-10 dataset to provide conformal prediction guarantees with non-conformity scores as given in (10). The goal is to assess the reliability of classification predictions by determining a threshold of non-conformity scores that covers 95% of the data.

To achieve this, non-conformity scores are obtained for all classes, and a threshold is calculated such that it contains 95% of the data. This threshold determines the coverage of the classification, which refers to the proportion of predictions that actually contain the true outcome.

This prediction threshold is determined by finding the percentile corresponding to  $1 - \alpha$ , where  $\alpha$  is set to 0.05 to achieve 95% coverage. Fig. 8(a) shows the non-conformity scores for all the calibration data,  $j = 1000$  [4] (using the following split: 40000:10000:9000:1000 training, testing, validation and calibration data points respectively for CIFAR-10), with a cut-off threshold that ensures 95% coverage.

The conformal prediction sets for two sample inputs are shown in Fig. 7, along with their predicted probabilities.

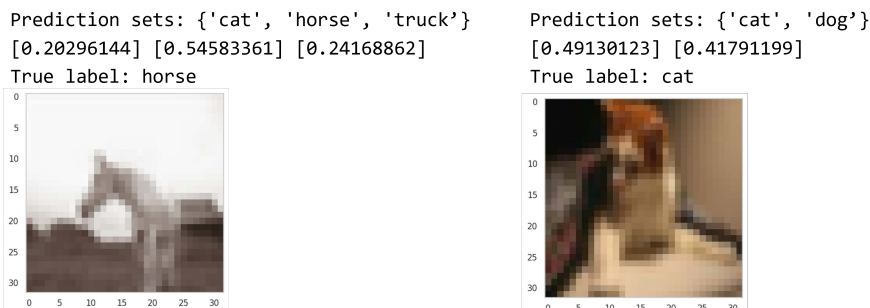


Figure 7: Conformal prediction sets by RS-NN on the CIFAR-10 dataset. The predicted probabilities for each class is shown.

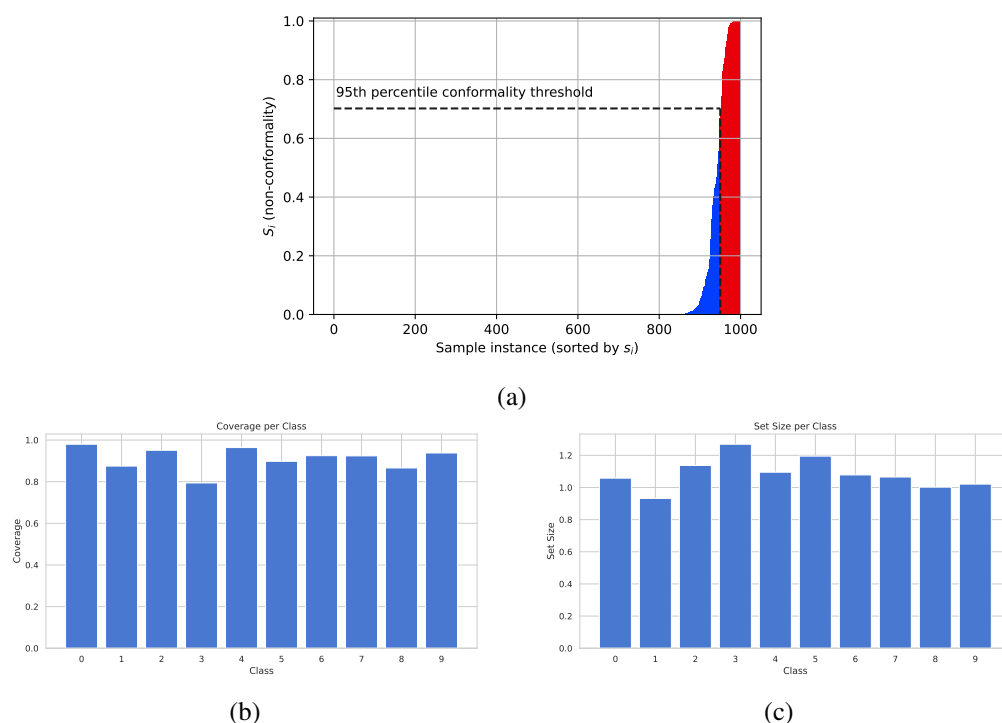


Figure 8: (a) Conformal prediction threshold for CIFAR-10 indicating the boundary beyond which predictions are considered non-conformal, (b) Coverage per class for CIFAR-10 dataset, representing the proportion of instances in each class that fall within the predictive regions, (c) Average size of the predictive sets generated for each class of CIFAR-10.

Figs. 8(b) and 8(c) show the coverage and average set size for each class on the test dataset. Coverage is the proportion of prediction sets that actually contain the true outcome, and average set size is the average number of predicted classes per instance. Higher numbers represent more overlap between the classification regions of different classes.

Summarizing the results, (1) the coverage averages across classes over the desired threshold. This indicates that the conformal prediction method is providing reliable prediction intervals that contain the true class label with the specified confidence level; (2) The spread or variability in set sizes across different samples provides insights into how well the prediction sets adapt to the difficulty of the samples. Ideally, the prediction sets should dynamically adjust based on the difficulty of each example, with larger sets for more challenging inputs and smaller sets for easier ones. Fig. 8(c) shows that the average set size for classes 1, 2, 3, 4, and 6 is considerably larger than for the rest, indicating that the model found samples from these as challenging inputs.

**Alternative approaches to statistical guarantees.** In the future we plan to explore the possibility of generalising the empirical CDF at the basis of conformal learning in a belief function / random set representation, aiming to retain statistical guarantees. Given the complexity of this enterprise, we are working towards this in a separate paper.

Finally, an intriguing alternative approach (and one that is more achievable in the short term) is the study of confidence intervals in a belief functions representation, such as the one we employ in RS-NNs. In fact, recent studies have been looking at extending the notion of confidence interval ([https://en.wikipedia.org/wiki/Confidence\\_interval](https://en.wikipedia.org/wiki/Confidence_interval)) to belief functions, under the name of *confidence structures* (<https://hal.science/hal-01576356v3>), which generalise standard confidence distributions and generate “frequency-calibrated” belief functions.

Liu and Martin, in particular, have developed an Inferential Model (IM) approach which produces belief functions with well-defined frequentist properties [71, 72]. An alternative approach relies on the notion of “predictive” belief function [26], which, under repeated sampling, is less committed than the true probability distribution of interest with some prescribed probability.

### A.3 RS-NN Learning Mechanism

Recall from Sec. 3.1 that the ground-truth for a Random Set-CNN is the belief-encoded vector  $\mathbf{bel} = \{Bel(A), A \in \mathbb{P}(\mathcal{C})\}$ , where  $Bel(A)$  is the belief function of a focal set  $A$  in the power set  $\mathbb{P}$  of classes  $\mathcal{C}$ . In our method,  $Bel(A)$  is 1 if the true class is in subset  $A$  and 0 otherwise. Consequently, the belief-encoded ground truth  $\mathbf{bel}$  will include multiple occurrences of 1. For instance, in a digit-classification task such as MNIST, if  $\{3\}$  is the true class, the belief-encoded ground truth would contain 1s in all sets where  $\{3\}$  is present, such as  $\{1, 3\}$ ,  $\{0, 3\}$ ,  $\{1, 2, 3\}$ , and so forth. This formulation closely resembles multi-label classification.

Since we assign precise labels for belief containing different focal sets, our model begins by penalizing predictions that differ from the observed label in the same manner, regardless of the set’s composition or relationship to the true label. Using MNIST as an example, this means that the loss incurred for predicting label  $\{3\}$  is equivalent to predicting label  $\{3, 7\}$ , as both sets contain the true label. This equivalence in losses might seem counterintuitive at first glance. However, despite the identical loss values, the probabilities output by the sigmoid activation function will vary due to differences in the input logit values for each label. For instance, if the correct label is  $\{3\}$ , the loss for predicting  $\{3\}$  or  $\{3, 7\}$  would be the same. Still, the loss for predicting  $\{7\}$  would differ, allowing the model to discern the set structure during training.

During the training process, the model learns to capture and understand these relationships by observing patterns and dependencies in the training data. As the model optimizes its parameters based on the training objective (e.g., minimizing the loss function), it gradually adjusts its internal representations to better reflect these relationships. We use as the basis for our loss function Binary cross-entropy with sigmoid activation. It allows the model to predict the presence or absence of each label separately as a binary classification problem, producing probabilities between 0 and 1 for each class. While the model is unaware that it is learning for sets of outcomes, we leverage this technique to extract mass functions and pignistic predictions from the learnt belief functions. By re-distributing masses to original classes, we obtain the best pignistic predictions that are often more accurate than standard CNN predictions, attributing to the higher accuracy in Tab. 2.

### A.4 Pignistic probability and credal prediction

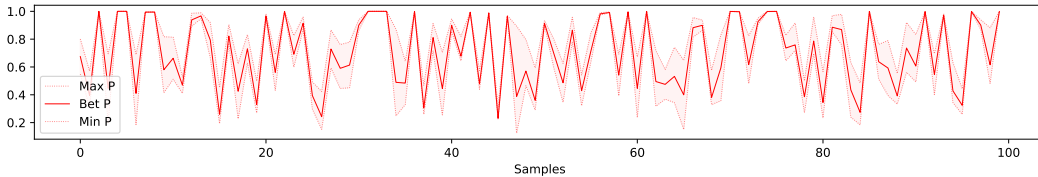


Figure 9: Upper and lower bounds (9), in dotted red, to the probability of the predicted most likely class according to the pignistic prediction (in solid red) for 100 samples of CIFAR-10.

For additional illustration, the lower and upper bounds (9) to the probability of the top predicted class are plotted in Fig. 9, together with the pignistic probability, for 100 samples of CIFAR-10. The

bounds (9) can be efficiently computed from the finite number of vertices of the credal prediction ([18], Fig. 4).

## B Related Work

Researchers have recently taken some tentative steps to model uncertainty in machine learning and artificial intelligence. Scientists have adopted measures of epistemic uncertainty [56] to refuse or delay making a decision [39], take actions specifically directed at reducing uncertainty (as in active learning [2]), or exclude highly-uncertain data at decision making time [56].

**Imprecise probability.** Significant work has been done in a credal set setting. Notably, [113, 17] have proposed the Naive Credal Classifier (NCC) as an extension of the naive Bayes classifier to credal sets, where imprecise probabilities are included in models in the form of sets of classes. [5] have presented graphical models which generalise NCCs to multilabel data. Expected utility maximisation algorithms, such as Bayes-optimal prediction [76], and classification with reject option for risk aversion [80] are also based on set-valued predictions. Classification with partial data has been studied by various authors [104], while a large number of papers have been published on decision trees in the belief function framework [32]. Significant work in the neural network area was conducted in [25] and [33]. Classification approaches based on rough sets were proposed in [101]. Ensemble classification [13] is another area in which uncertainty theory has been quite impactful, as the problem is one of combining the results of different classifiers. Important contributions have been made by [112] and [88]. Regression, on the other hand, has only recently been considered by belief theorists [65, 42, 28]. For tasks like image classification in large datasets, most of these approaches have low performance metrics including training time and test accuracy. The epistemic deep learning approach utilizes standard networks to achieve better performance.

**Evidential approaches.** Within a proper epistemic setting, a significant amount of work has been done by Denoeux and co-authors, and Liu et al. [36], on unsupervised learning and clustering in particular in the belief function framework. Quite a lot of work has been done on ensemble classification in the evidential framework [112] (in particular for neural networks [88]), decision trees [31], K-nearest neighbour classifiers [27], and more recently on evidential deep learning classifiers able to quantify uncertainty [100]. Tong et al.[100] proposes a convolutional neural network based on Dempster-Shafer theory called the evidential deep-classifier employs utility functions from decision theory to assign utilities on mass functions derived from input features to produce set-valued observations. Another recent approach by Sensoy et al.[92] proposes an evidential deep learning classifier to estimate uncertainty in the Dirichlet representation. This work is based on subjective logic and learning to form subjective opinions by minimizing the Kullback-Leibler divergence over a uniform Dirichlet distribution. However, epistemic deep learning does not depend on evidence-based parameters for learning.

**Conformal prediction.** Conformal prediction [106] provides a framework for estimating uncertainty [94] by applying a threshold on the error the model can make to produce prediction sets, irrespective of the underlying prediction problem. Different variants of conformal predictors are described in papers by Saunders et al. [91], Nouretdinov et al. [81], Proedrou et al. [87] and Papadopoulos et al. [83]. Since the computational inefficiency of conformal predictors posed a problem for their use in neural networks, Inductive Conformal Predictors (ICPs) were proposed by Papadopoulos et al. [84] [85]. Venn Predictors [108], cross-conformal predictors [105] and Venn-Abers predictors [107] were introduced in distribution-free uncertainty quantification using conformal learning.

## C Algorithms

### C.1 Algorithm for Budgeting

For RS-NN with  $N$  classes, generating  $2^N$  outputs is computationally infeasible due to exponential complexity. Instead, we choose  $K$  relevant subsets ( $A_K$  focal sets) from the  $2^N$  possibilities.

To obtain these  $K$  focal subsets, we extract feature vectors from the penultimate layer of a trained standard CNN with  $N$  outputs. We then apply t-SNE for dimensionality reduction to 3 dimensions. Note that our approach is agnostic, as t-SNE could be replaced with any other dimensionality reduction technique, including autoencoders.

---

**Algorithm 1** Budgeting Algorithm

---

```
1: Input:  $\mathcal{D}$  – Training data with  $N$  classes,  $\mathcal{C}$  – The set of classes,  $K$  – Number of non-singleton focal sets
2: Output:  $\mathcal{O}$  – Set containing  $N + K$  focal sets
3: Initialization
4: Extract feature vectors using a trained CNN
5: Apply t-SNE for dimensionality reduction to 3 dimensions
6: for each class  $c$  do
7:   Fit GMM to the reduced feature vectors for that class to obtain  $\mu_c$  and  $\Sigma_c$ 
8:   Define an ellipsoid covering 95% data using  $\mu_c$  and  $\Sigma_c$ 
9: end for
10:  $\text{most\_overlapping\_sets} \leftarrow$  Initialize an empty list for non-singleton focal sets  $A_1, \dots, A_K$ 
11: Set  $\text{current\_cardinality} \leftarrow 2$ 
12: while  $\text{current\_cardinality} \leq N$  do
13:   Compute overlaps for subsets of cardinality current_cardinality
14:    $\text{overlap}(A) = \frac{\bigcap_{c \in A} A^c}{\bigcup_{c \in A} A^c}$ 
15:   Select top-K subsets with highest overlap
16:   Update  $\text{most\_overlapping\_sets}$ 
17:   if no change in  $\text{most\_overlapping\_sets}$  then
18:     break
19:   end if
20:    $\text{current\_cardinality} \leftarrow \text{current\_cardinality} + 1$ 
21: end while
22: Combine selected non-singleton focal sets with  $N$  singleton sets
23:  $\mathcal{O} \leftarrow \mathcal{C} \cup \{A_1, \dots, A_K\}$ 
24: return  $\mathcal{O}$ 
```

---

Next, we fit a Gaussian Mixture Model (GMM) to the reduced feature vectors of each class. Using the eigenvectors and eigenvalues of the covariance matrix  $\Sigma_c$  and the mean vector  $\mu_c$  for each class  $c$ , we define an ellipsoid covering 95% of the data. The lengths of the ellipsoid’s principal axes are computed as  $\text{length}_{c,i} = 2\sqrt{7.815\lambda_i}$ , where  $\lambda_i$  is the  $i^{\text{th}}$  eigenvalue. The scalar 7.815 corresponds to a 95% confidence interval. The class ellipsoids are plotted in a 3D space and the overlap of each subset in the power set of  $N$  is computed. As it is computationally infeasible to compute overlap for all  $2^N$  subsets, we start doing so from cardinality 2 and use early stopping when increasing the cardinality further does not alter the list of most-overlapping sets of classes. We choose the top- $K$  subsets ( $A_K$ ) with the highest overlapping ratio, computed as the intersection over union for each subset.

## C.2 Algorithm for ECE

Expected Calibration Error (ECE) is computed by comparing the average confidence and accuracy within each bin. The steps involved are as follows:

1. For each bin, calculate the absolute difference between the average confidence and the accuracy.
2. Weight each difference by the proportion of instances in that bin compared to the total number of instances.
3. Sum up these weighted differences across all bins to get the final ECE value.

The formula for ECE is given by:

$$\text{ECE} = \sum_{i=1}^B |(\text{Accuracy}_i - \text{Confidence}_i)| \times \text{Weight}_i$$

where:

- $\text{Accuracy}_i$  is the accuracy within the  $i$ -th bin.
- $\text{Confidence}_i$  is the average confidence within the  $i$ -th bin.

---

**Algorithm 2** Expected Calibration Error (ECE)

---

**Require:** *confidences*: List or array of confidence scores predicted by the model *predictions*: List or array of predicted class labels *true\_labels*: List or array of true class labels *B*: Number of bins for binning confidence scores

**Ensure:** *ECE*: Expected Calibration Error

- 1: **Step 1: Normalize Confidences** Normalize the confidence scores to ensure they are in the range  $[0, 1]$ .
- 2: **Step 2: Binning** Divide the confidence scores into *num\_bins* bins.
- 3: **Step 3: Initialize Arrays** Initialize arrays *bin\_accuracy*, *bin\_confidence*, and *weights* with zeros.
- 4: **Step 4: Populate Arrays**
- 5: **for each bin do**
- 6:   Identify instances falling into the bin
- 7:   Calculate mean accuracy and mean confidence within the bin
- 8:   Update *bin\_accuracy*, *bin\_confidence*, and *weights*
- 9: **end for**
- 10: **Step 5: Calculate ECE** Calculate the Expected Calibration Error using the populated arrays.

$$ECE = \sum_{i=1}^B |(bin\_accuracy_i - bin\_confidence_i)| \times weights_i$$

---

- $Weight_i$  is the proportion of instances in the  $i$ -th bin compared to the total number of instances.
- $B$  is the total number of bins.

The final ECE value represents how much the model’s estimated probabilities differ from the true (observed) probabilities. A low ECE indicates well-calibrated probabilistic predictions, demonstrating that the model’s confidence scores align closely with the actual likelihood of events. RS-NN exhibits the lowest ECE as shown in Tab 1.

### C.3 Algorithm for AUROC, AUPRC

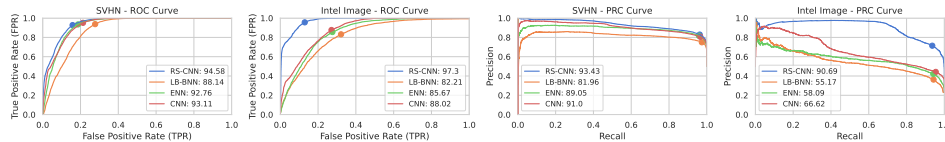


Figure 10: Receiver Operating Characteristic (ROC) and Precision-Recall Characteristic (PRC) curves for RS-NN, LB-BNN, ENN, and CNN evaluated on the SVHN and Intel Image OoD datasets for CIFAR-10.

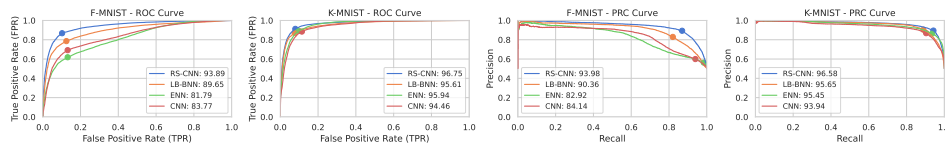


Figure 11: Receiver Operating Characteristic (ROC) and Precision-Recall Characteristic (PRC) curves for RS-NN, LB-BNN, ENN, and CNN evaluated on the SVHN and Intel Image OoD datasets for MNIST.

Out-of-distribution (OoD) detection involves the identification of data points that deviate from the in-distribution (iD) data on which a model was trained. This process relies on assessing the model’s uncertainty, particularly its epistemic uncertainty, which reflects the model’s lack of knowledge or confidence in making predictions. When exposed to OoD data, which differs significantly from the training data, the model tends to exhibit higher epistemic uncertainty.

---

**Algorithm 3** Algorithm for AUROC, AUPRC

---

**Require:** *uncertainty\_iid*: Uncertainty scores for in-distribution samples. *uncertainty\_ood*: Uncertainty scores for out-of-distribution samples.

**Ensure:** (fpr, tpr, thresholds): ROC curve metrics.  
(precision, recall, prc\_thresholds): Precision-Recall curve metrics.  
auroc: Area Under the Receiver Operating Characteristic curve.  
auprc: Area Under the Precision-Recall curve.

- 1: **Step 1: Concatenate uncertainties;**  
uncertainties  $\leftarrow$  concatenate(uncertainty\_iid, uncertainty\_ood)
  - 2: **Step 2: Create and combine labels;**  
in\_labels  $\leftarrow$  zeros(uncertainty\_iid.shape[0]) ood\_labels  $\leftarrow$  ones(uncertainty\_ood.shape[0])  
labels  $\leftarrow$  concatenate(in\_labels, ood\_labels)
  - 3: **Step 4: Calculate ROC curve;**  
(fpr, tpr, thresholds)  $\leftarrow$  roc\_curve(labels, uncertainties)
  - 4: **Step 5: Calculate AUROC;**  
auroc  $\leftarrow$  roc\_auc\_score(labels, uncertainties)
  - 5: **Step 6: Calculate Precision-Recall curve;**  
(precision, recall, prc\_thresholds)  $\leftarrow$  precision\_recall\_curve(labels, uncertainties)
  - 6: **Step 7: Calculate AUPRC;**  
auprc  $\leftarrow$  average\_precision\_score(labels, uncertainties)
- 

AUROC (Area Under the Receiver Operating Characteristic Curve) and AUPRC (Area Under the Precision-Recall Curve) are evaluation metrics commonly used to assess the performance of binary classification models, providing insights into their ability to distinguish between positive and negative instances. In the context of evaluating uncertainty estimation in machine learning models, these metrics quantify how well the model separates iD samples from OoD samples. AUROC is derived from the Receiver Operating Characteristic (ROC) curve, which illustrates the trade-off between True Positive Rate (TPR) and False Positive Rate (FPR) across various classification thresholds. The AUROC value represents the area under this curve and ranges from 0 to 1, with higher values indicating better discriminative performance. AUPRC is based on the Precision-Recall curve, which plots Precision against Recall at different classification thresholds. Precision measures the accuracy of positive predictions, while Recall quantifies the ability to capture all positive instances. AUPRC calculates the area under this curve and provides a complementary perspective, particularly valuable when dealing with imbalanced datasets.

Figs. 10 and 11 plot each model’s performance, illustrating the trade-offs between True Positive Rate and False Positive Rate (ROC curve), Precision and Recall (PRC curve) for CIFAR-10 (Fig. 10) and MNIST (Fig. 11). The left two plots depict the AUROC curves, where the blue curve representing RS-NN outperforms others, indicating superior discrimination between true positive and false positive rates. Similarly, on the two right plots displaying Precision-Recall Curve (PRC), RS-NN exhibits the highest curve, emphasizing its precision and recall performance. These results showcase RS-NN’s effectiveness in distinguishing in-distribution and out-of-distribution samples.

## D Additional Experimental results

### D.1 Robustness to noisy data

We split the MNIST data into training and test sets, train the RS-NN model using the training test, and test the model on noisy and rotated out-of-distribution test data. This is done by adding random noise to the test set of images to obtain noisy data and rotating MNIST images with random degrees of rotation between 0 and 360.

Tab. 5 shows the test accuracies for standard CNN, RS-NN, LB-BNN and ENN at different scales of random noise. RS-NN shows significantly higher test accuracy than other models as the amount of noise added to the test data increases.

The test accuracies for standard CNN, RS-NN, LB-BNN and ENN on Rotated MNIST images are shown in Tab 6. The samples are randomly rotated every 60 degrees,  $-180^\circ$  to  $-120^\circ$ ,  $-120^\circ$  to  $-60^\circ$ ,

Table 5: Test accuracies(%) for RS-NN, standard CNN, LB-BNN (Bayesian) and ENN (Ensemble) on noisy samples of MNIST . ‘Scale’ represents the standard deviation of the normal distribution from which random numbers are being generated for random noise.


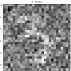
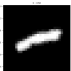
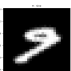
Noise (scale)	0.2	0.3	0.4	0.5	0.6	0.7	0.8
Standard CNN	93.40%	79.08%	79.15%	58.33%	40.19%	28.15%	28.59%
RS-NN	96.90%	85.36%	<b>85.91</b> %	<b>68.33</b> %	<b>51.46</b> %	<b>37.18</b> %	<b>38.05</b> %
LB-BNN	<b>98.47%</b>	<b>95.26</b> %	80.18%	61.56%	43.28%	31.41%	24.55
ENN	97.81%	90.76%	75.41%	58.99%	45.70%	36.97%	31.51

-60° to 0°, etc. A fully random rotation between 0° and 360° also shows higher test accuracy for RS-NN at 47.71% when compared to standard CNN with test accuracy 45.86%.

Table 6: Test accuracies(%) for RS-NN, standard CNN, LB-BNN (Bayesian) and ENN (Ensemble) on Rotated MNIST out-of-distribution (OoD) samples. Rotation angle is random between the values given.

Rotation (angle)	-180/-120	-120/-60	-60/0	0/60	60/120	120/180	0/360
Standard CNN	36.41%	21.86%	74.41%	80.80%	23.89%	37.53%	45.86%
RS-NN	<b>37.84%</b>	<b>23.54%</b>	<b>78.44%</b>	<b>81.46%</b>	<b>26.31%</b>	<b>38.48%</b>	<b>47.71%</b>
LB-BNN	37.56%	20.19%	75.12%	77.67%	23.18%	37.83%	46.07
ENN	36.40%	19.43%	71.70%	78.59%	18.70%	36.38%	44.14

Table 7: Standard CNN fails to perform well when tested on noisy noisy and rotated samples of MNIST test data. The predicted results show how a standard CNN predicts the wrong class with a high confidence score, whereas the RS-NN model predicts the right class with varying confidence scores.

		Standard CNN Predictions	Belief	RS-NN Predictions			
<b>True Label = 2</b>							
	<b>Class 0</b>	<b>0.628</b>		<b>Belief values</b>	<b>Mass values</b>	<b>Pignistic</b>	
	Class 2	0.232	{‘2’}	0.985	{‘2’}	0.982	<b>2 0.982</b>
	Class 3	0.117	{‘2’, ‘0’, ‘1’}	0.981	{‘0’, ‘8’}	0.009	8 0.007
	Class 8	0.015	{‘2’, ‘1’}	0.980	{‘7’, ‘0’, ‘1’}	0.002	0 0.100
			{‘2’, ‘4’}	0.979	{‘7’, ‘8’}	0.002	3 0.004
<b>True Label = 3</b>							
	<b>Class 8</b>	<b>0.969</b>		<b>Belief values</b>	<b>Mass values</b>	<b>Pignistic</b>	
	Class 5	0.018	{‘3’, ‘5’}	0.772	{‘3’}	0.361	<b>3 0.427</b>
	Class 9	0.006	{‘6’, ‘3’}	0.637	{‘7’, ‘8’}	0.134	8 0.205
	Class 2	0.003	{‘6’, ‘3’, ‘5’}	0.620	{‘0’, ‘8’}	0.104	5 0.115
			{‘3’}	0.540	{‘8’}	0.084	7 0.080
<b>True Label = 1</b>							
	<b>Class 2</b>	<b>1.0</b>		<b>Belief values</b>	<b>Mass values</b>	<b>Pignistic</b>	
	Class 1	3.39e-08	{‘2’, ‘1’}	0.999	{‘1’}	0.556	<b>1 0.566</b>
	Class 6	1.03e-10	{‘1’, ‘9’}	0.958	{‘2’}	0.423	2 0.423
	Class 3	4.92e-11	{‘1’}	0.924	{‘1’, ‘9’}	0.020	9 0.010
			{‘1’, ‘5’}	0.825	{‘6’}	4.31e-05	6 4.31e-05
<b>True Label = 9</b>							
	<b>Class 5</b>	<b>0.988</b>		<b>Belief values</b>	<b>Mass values</b>	<b>Pignistic</b>	
	Class 2	0.010	{‘7’, ‘5’, ‘9’}	0.831	{‘7’, ‘9’}	0.171	<b>9 0.699</b>
	Class 3	0.0004	{‘7’, ‘9’}	0.706	{‘3’}	0.134	7 0.023
	Class 7	0.0002	{‘5’, ‘9’}	0.576	{‘9’}	0.132	5 0.004
			{‘3’, ‘9’}	0.558	{‘7’, ‘8’}	0.102	3 0.001

Tab 7 shows predictions for noisy and rotated noisy MNIST samples. In cases where a standard CNN makes wrong predictions with high confidence scores, Random-Set NN manages to predict the correct class with varying confidences verifying that the model is not overconfident in uncertain cases. For example, a noisy sample with true class ‘3’ has a standard CNN prediction of class ‘8’ with



96.9% confidence, while RS-NN predicts the correct class {‘3’} with 42.7% confidence. Similarly, for rotated ‘9’, the standard CNN predicts class ‘5’ with 98.8% confidence whereas RS-NN predicts the correct class {‘9’} with 69.9% confidence. For a rotated ‘1’, the standard CNN predicts class ‘2’ with 100% confidence.

## D.2 Robustness to adversarial attacks

We conducted experiments on adversarial attacks using the well-known Fast Gradient Sign Method (FGSM) [43]. FGSM is a popular approach for generating adversarial examples by perturbing input images based on the sign of the gradient of the loss function with respect to the input. Mathematically, the perturbed image  $x'$  is computed as

$$x' = x + \epsilon \cdot \text{sign}(\nabla_x J(\theta, x, y)), \tag{11}$$

where  $x$  is the original input image,  $\epsilon$  (epsilon) is a small scalar representing the magnitude of the perturbation,  $J$  is the loss function,  $\theta$  are the model parameters, and  $y$  is the true label of the input image.

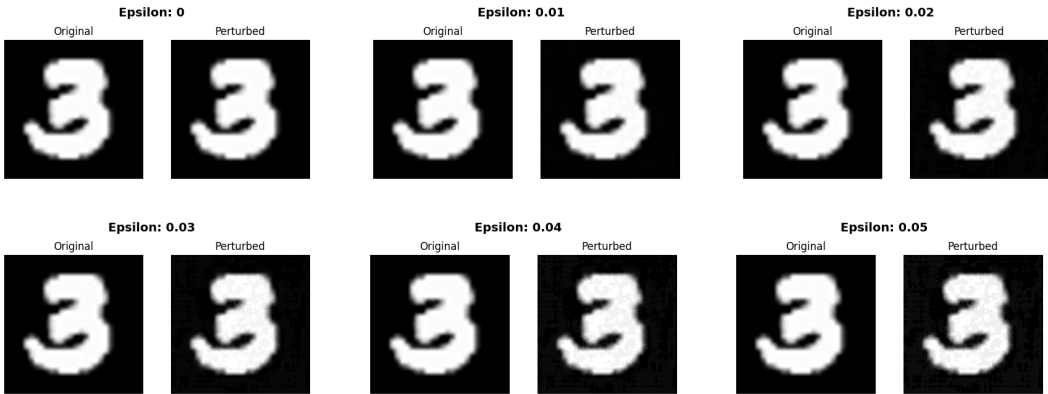


Figure 12: Examples of perturbed images generated using FGSM adversarial attacks on the MNIST dataset for different epsilon values. Epsilon values range from 0 to 0.05.

In our experiments, we applied FGSM adversarial attacks on the MNIST dataset for both standard CNN and Random-Set NN (RS-NN) models. This involved perturbing images from the MNIST dataset with noise generated using FGSM based on the gradient of the loss function (namely, the cross entropy loss for CNN and the  $\mathcal{L}_{B-RS}$  loss, see Sec. 3.2, (7), for RS-NN).

Table 8: Test accuracies of CNN and RS-NN models under FGSM adversarial attacks on the MNIST dataset for different epsilon values. Epsilon values range from 0 to 0.05.

Model		Epsilon ( $\epsilon$ )						
		0	0.005	0.01	0.02	0.03	0.04	0.05
Test acc. (%)	CNN	98.90	98.25	94.82	72.62	49.75	38.08	32.43
	RS-NN	<b>99.17</b>	<b>98.46</b>	<b>95.84</b>	<b>91.90</b>	<b>90.62</b>	<b>90.10</b>	<b>89.72</b>

Subsequently, we evaluated the models’ predictions on these perturbed images and computed their test accuracies. Tab. 1 in the anonymous PDF linked to this response presents the test accuracies of both CNN and RS-NN models under FGSM adversarial attacks on the MNIST dataset for different values of  $\epsilon$ . As can be observed there, RS-NN demonstrates significantly higher robustness to these adversarial attacks compared to CNN, showcasing its superior resilience to adversarial perturbations. For additional information, Fig. 1 in the PDF shows examples of perturbed images generated using FGSM adversarial attacks applied to the MNIST dataset for various epsilon values ranging from 0 to 0.05.

### D.3 Overconfidence in CNNs

Tab 9 shows an noisy example of a rotated MNIST image with a true label ‘8’. The standard CNN makes an incorrect prediction (‘6’) with 99.95% confidence and a low entropy of 0.0061, showcasing a noTab limitation in relying solely on confidence scores and entropy of predicted probabilities. RS-NN provides a correct prediction (class ‘8’) with a confidence of 49.7% and pignistic entropy of 2.1626 and a credal set width of 0.482. Crucially, the RS-NN’s prediction process considers more than just the predicted class, taking into account both the confidence of the pignistic probability and the entropy. In this example, despite predicting the correct class (‘8’), the RS-NN demonstrates a low confidence (49.7%) and high entropy (2.1626). This holistic approach provides a more nuanced and reliable understanding of the model’s uncertainty,

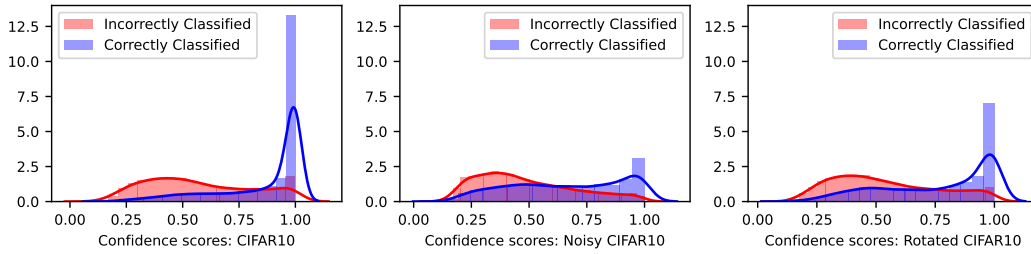


Figure 13: Confidence scores of RS-NN on CIFAR-10, Noisy CIFAR-10, and Rotated CIFAR-10

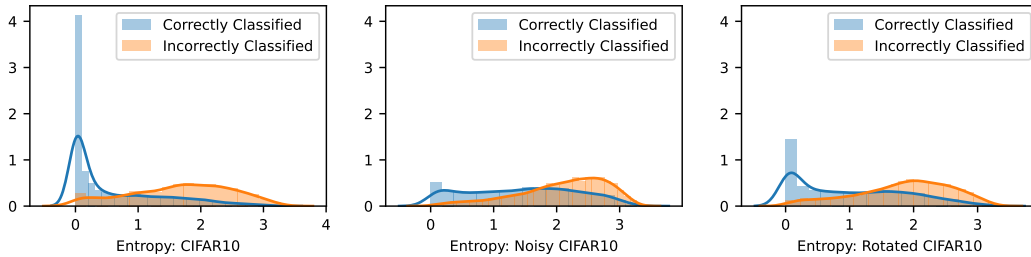



Figure 14: Entropy distribution of RS-NN on CIFAR-10, Noisy CIFAR-10, and Rotated CIFAR-10

Table 9: Standard CNN fails to perform well when tested on an noisy (rotated) sample of MNIST test data. The predicted results show how a standard CNN predicts the wrong class with a high confidence score (99.95%), while the RS-NN model predicts the correct class with 49.7% confidence and a high entropy of 2.1626.

True Label = "8"	CNN Predictions	RS-NN Predictions				
	Class 6	0.9995	Belief values		Pignistic Probability	
	Class 5	0.0002	{'6', '4', '8'}	0.7853	{'6', '8'}	<b>8</b> 0.4978
	Class 8	0.0001	{'6', '8', '1'}	0.7150	{'9', '8', '1'}	6 0.2294
	Class 0	1.4e-05	{'6', '8'}	0.6357	{'8'}	9 0.1002
	Class 4	1.1e-06	{'9', '8'}	0.5529	{'8', '3'}	3 0.0502
			{'8', '3'}	0.4092	{'6'}	4 0.0459
	Entropy 0.0061	Entropy 2.1626	Credal set width 0.582			

A distribution of confidence scores for RS-NN in the same noisy experiment are shown in Fig. 13 for both incorrectly classified and correctly classified samples. In Fig. 15, we show how a standard CNN has high confidence for incorrectly classified samples whereas RS-NN exhibits lower confidence and higher entropy (Fig. 14) for incorrectly classified samples. Fig. 14 displays the entropy distribution for correctly and incorrectly classified samples of CIFAR-10, including in-distribution, noisy, and rotated images. Higher entropy is observed for incorrectly classified predictions across all three cases.

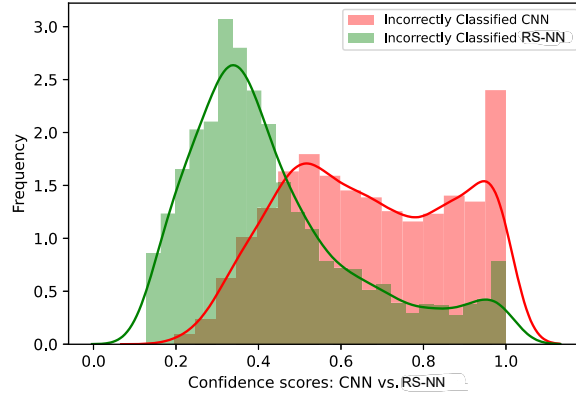


Figure 15: Confidence scores for *Incorrectly Classified samples* of RS-NN and CNN

#### D.4 Budgeting of sets

The budgeting procedure can also be modified to accommodate multiple data sources or a continuous stream of data. t-SNE can be replaced by an autoencoder (this will need to be trained first) or PCA to add continual inference capabilities in the dimensionality reduction step. Similarly, Gaussian-based dynamic probabilistic clustering (GDPC) [29] can be used instead of GMM clustering to handle a continuous stream of data. GDPC works by first initialising a GMM and then updating its parameters as it sees new data. In alternative, [64] have proposed an interesting approach to learn a GMM from multiple sources of data by maintaining a local and a global mixture model. Both these approaches can be plugged into our budgeting framework with little modifications to add continual learning capabilities to it. The computation of cluster overlaps remains the same, so overlapping scores and the resultant focal sets will need to be updated as the clusters evolve. However, a cluster tracking strategy [10] can be employed so that the overlap assessment step is only re-done when a sufficient drift has been detected in the clusters. All the proposed changes are efficient enough to not have a significant effect on the overall time of budgeting.

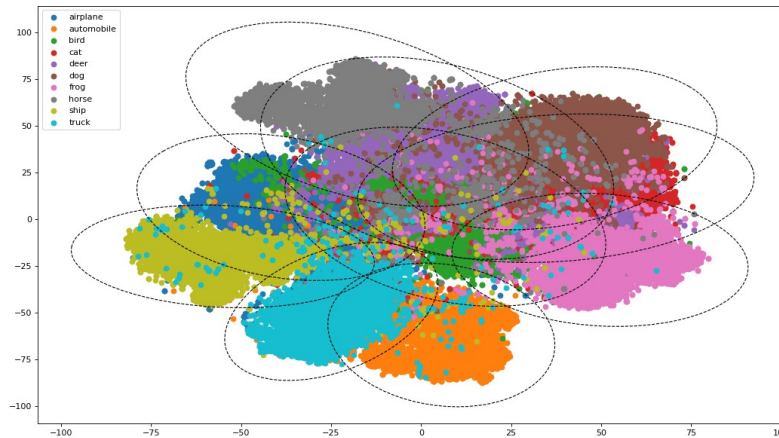


Figure 16: 2D visualization of the clusters of 10 classes of CIFAR-10 dataset and the ellipses formed by RS-NN based on the hyperparameters of Gaussian Mixture Models.

A 2D visualization of the ellipses formed by calculating the principle axes and their lengths using eigenvectors and eigenvalues obtained from GMMs, for each class  $c$  [99] is shown in Fig. 16.

## D.5 Uncertainty estimation for RS-NN

### D.5.1 Entropy vs Credal Set Width

Figs. 17 and 18 depict the relationship between the entropy of RS-NN pignistic prediction and the associated confidence level (Fig. 17), and between credal set width and confidence (Fig. 18) for the CIFAR-10 (left) and SVHN/Intel Image (right) datasets. The distribution of iD predictions (left) for both tests show a concentration at the top left, indicating high confidence and low entropy or credal set width. Conversely, OoD predictions (middle, right) exhibit a more dispersed pattern.

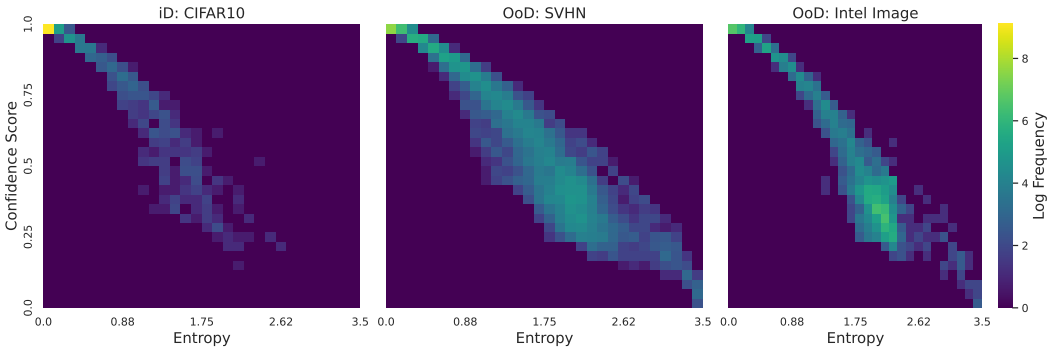


Figure 17: Entropy vs Confidence score on iD (left) vs OoD (right) datasets. For CIFAR-10, most predictions are concentrated top left of the plot indicating lower entropy and higher confidence in the predictions. For SVHN and Intel Image datasets, predictions are more distributed.

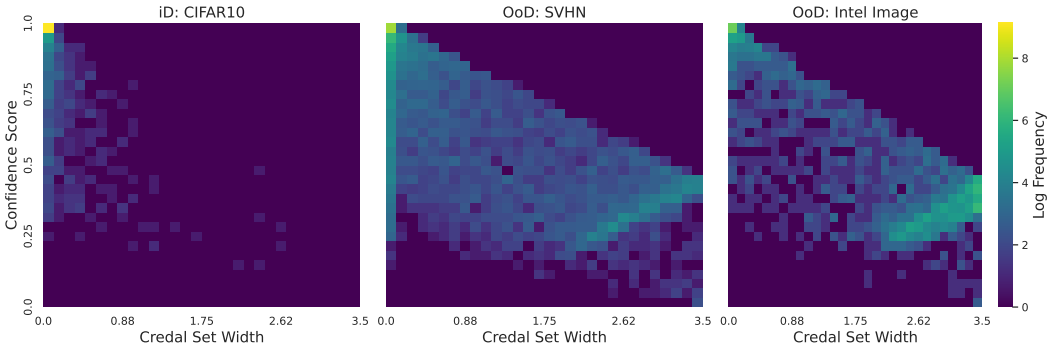


Figure 18: Credal Set Width vs Confidence score on iD (left) vs OoD (right) datasets. For CIFAR-10, confidence scores are high and credal set width is small. For SVHN and Intel Image datasets, credal set width varies for each prediction and is less reliant on confidence score.

Entropy, reflecting prediction uncertainty, is quite correlated with confidence, in both iD and OoD tests. In contrast, as it considers the entire set of plausible outcomes within a belief function rather than a single prediction, credal set width better quantifies the degree of epistemic uncertainty inherent to a prediction and, as a result, credal set width is less dependent on the concentration of predictions and is more reflective of the overall uncertainty encompassed by the model. Fig. 18 shows that, unlike entropy, credal width is clearly not correlated with confidence (Fig. 18).

### D.5.2 Qualitative results of entropy

Fig. 19 depicts entropy-based uncertainty estimates for rotated out-of-distribution (OoD) MNIST digit ‘3’ samples. All models accurately predict the true class at  $-30^\circ$ ,  $0^\circ$ , and  $30^\circ$ . RS-NN and LB-BNN consistently exhibit low entropy in these scenarios, while ENN shows higher entropy for correct classifications at these angles. As the rotation angle increases, indicating more challenging scenarios, all models predict the wrong class. Notably, LB-BNN fails to exhibit a significant increase in entropy for these incorrect predictions. ENN performs relatively better than RS-NN at  $60^\circ$  and  $90^\circ$  rotations but has previously demonstrated high entropy levels even for accurate predictions at

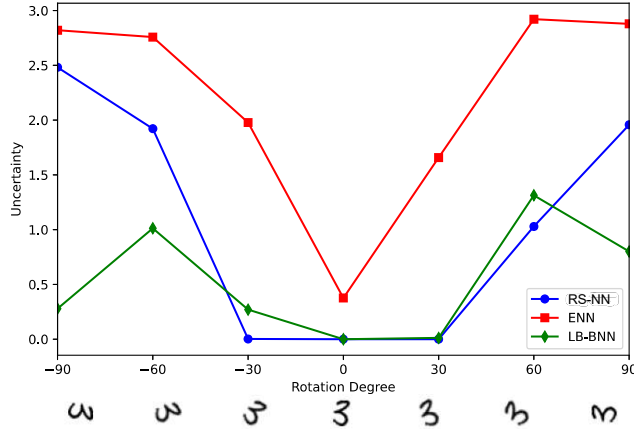


Figure 19: Uncertainty (entropy) of MNIST digit '3' rotated between -90 and 90 degrees. The blue line indicates RS-NN estimates low uncertainty between -30 to 30, and high uncertainty for further rotations.

relatively minor rotations of  $-30^\circ$  and  $+30^\circ$  degrees. Overall, RS-NN provides a more reliable measure of uncertainty.

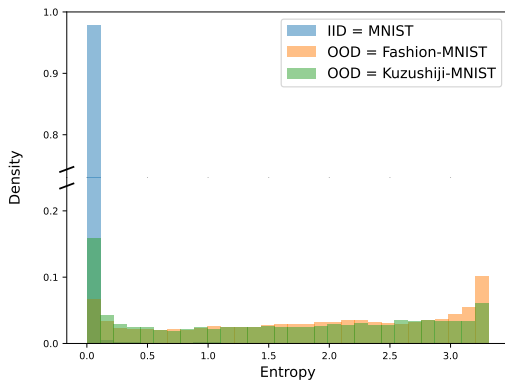


Figure 20: Entropy Distributions for RS-NN on MNIST vs Fashion-MNIST/Kuzushiji-MNIST.

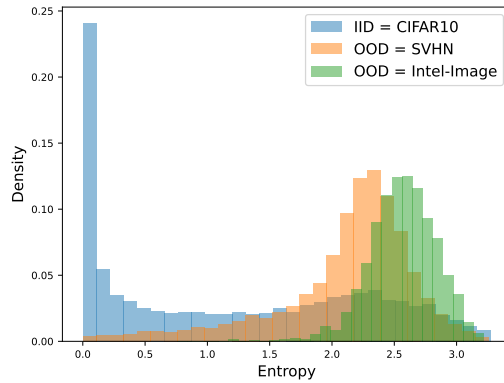


Figure 21: Entropy Distributions for RS-NN on CIFAR-10 vs SVHN/Intel-Image.

Figs. 20 and 21 show the entropy distributions for RS-NN on MNIST (iD) vs Fashion-MNIST (OoD)/Kuzushiji-MNIST (OoD), and CIFAR-10 (iD) vs SVHN (OoD)/Intel-Image (OoD), respectively. There is a clear iD vs OoD shift in entropy for RS-NN, as detailed in Sec. 4.4.

### D.5.3 Entropy of pignistic predictions

Tab 10 shows sample predictions by RS-NN: belief functions, masses, and pignistic predictions for given samples of CIFAR-10. The predicted belief, mass values, pignistic probabilities, and entropy are illustrated for two CIFAR-10 predictions. In the top figure, corresponding to the true label "horse," the model makes a highly confident prediction with 99.9% confidence and a low entropy of 0.0017. Conversely, the bottom figure, associated with the true label "cat," represents an uncertain prediction with 33.3% confidence and a higher entropy of 2.6955. It's important to note that the second image is slightly unclear and poor in quality.

Fig. 22 shows the entropy for two samples of CIFAR-10, one is a slightly uncertain image, whereas the other is certain with high belief values and lower entropy. Both results are shown for  $K = 20$  classes, additional to the 10 singletons.


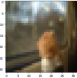
Sample	Belief	Mass	Pignistic	Entropy	
	{'horse', 'bird'} 0.9999402 {'horse', 'dog'} 0.9999225 {'horse'} 0.9999175 {'horse', 'deer'} 0.9998697 {'cat', 'truck'} 7.0380207e-05	{'horse'} {'cat', 'truck'} {'ship', 'bird'} {'horse', 'bird'} {'dog'}	0.9999175 6.859753e-05 4.094290e-05 2.250525e-05 1.717869e-05	horse 0.9998833 truck 3.5826409e-05 cat 3.3859180e-05 bird 3.3015738e-05 ship 2.3060647e-05	0.0017040148
	{'deer', 'cat'} 0.4787728 {'deer', 'airplane', 'bird'} 0.4126398 {'horse', 'deer'} 0.3732957 {'deer', 'bird'} 0.3658997 {'deer', 'dog'} 0.3651531	{'deer'} {'cat', 'truck'} {'dog', 'bird'} {'horse', 'bird'} {'bird'}	0.3104962 0.1762222 0.0998060 0.0954350 0.0524873	deer 0.3332411 cat 0.2230723 horse 0.1153417 bird 0.1086245 dog 0.1039505	2.6955228261

Table 10: The predicted belief, mass values, pignistic probabilities, and entropy for two CIFAR-10 predictions. The figure on the top (True Label = "horse") is a certain prediction with 99.9% confidence and a low entropy of 0.0017, whereas the figure on the bottom (True Label = "cat") is an uncertain prediction with 33.3% confidence and a higher entropy of 2.6955.

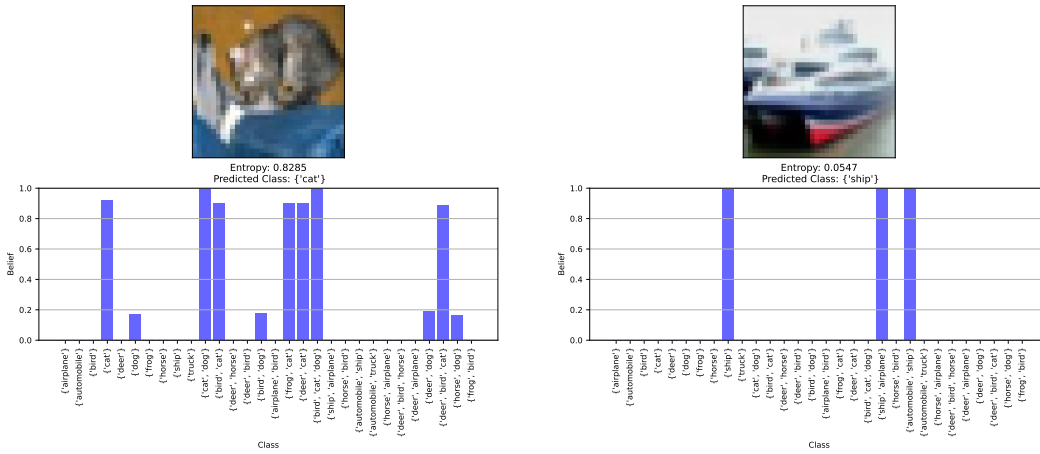


Figure 22: Entropy, predicted class and belief value graph for two samples of CIFAR-10 dataset.

#### D.5.4 Credal set width

Fig. 23 plots the credal set widths for incorrectly classified (left) and correctly classified (right) samples over each class  $c$  in CIFAR-10, respectively. The box represents the interquartile range between the 25th and 75th percentiles of the data encompassing most of the data. The vertical line inside the box represents the median and the whiskers extend from the box to the minimum and maximum values within a certain range, and data points beyond this range are considered outliers and are plotted individually as dots or circles. The box plots here are shown for 10,000 samples of CIFAR-10 dataset where most samples within the incorrect classifications have higher credal set widths indicating higher uncertainty in these samples, especially for classes 'bird', 'cat', 'deer', and 'dog'.

#### D.5.5 Ablation study on hyperparameters

As we discussed in the main paper, the regularization serves the purpose of ensuring that our model generates valid belief functions, which are constrained by maintaining a sum of masses equal to 1 and ensuring non-negativity. These terms are designed to penalize deviations from valid belief functions. However, it is crucial not to assign too much weight to this term, as excessively penalizing deviations may hinder the model's ability to accurately classify data points. For example, in a Variational Auto Encoder (VAE), if we assign too much weight to the KL divergence term in the loss, the model may prioritize fitting the latent distribution at the expense of reconstructing the input data accurately. This imbalance can lead to poor reconstruction quality and suboptimal performance on downstream tasks.

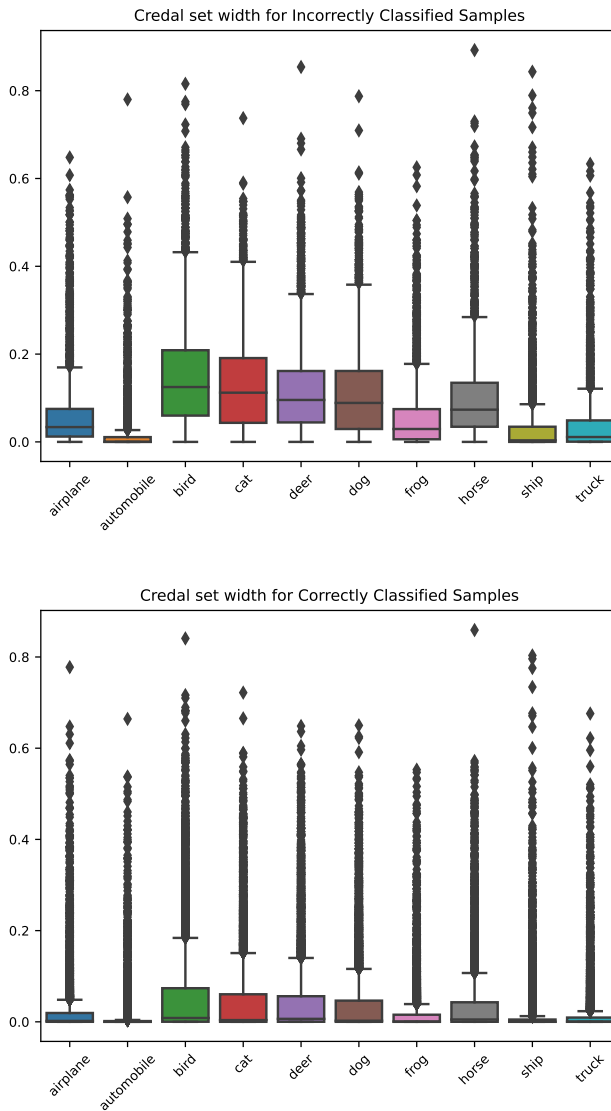


Figure 23: Credal set widths for individual classes of CIFAR-10 dataset. For Incorrectly Classified samples (*top*). For Correctly Classified samples (*bottom*).

Hence, it is essential to properly tune the values of  $\alpha$  and  $\beta$  to ensure that these regularization terms play a meaningful role in the training. The ablation study on hyperparameters is conducted to examine the impact of  $\alpha$  and  $\beta$  on the model’s accuracy. It demonstrates that small values suffice for these parameters.

In Fig. 24, we show the test accuracies for different values of hyperparameters  $\alpha$  and  $\beta$  in  $\mathcal{L}_{B-RS}$  loss function (7). Hyperparameters  $\alpha$  and  $\beta$  adjusts the relative significance of the regularization terms  $M_r$  and  $M_s$  respectively in  $\mathcal{L}_{B-RS}$  loss. The test accuracies are calculated for CIFAR-10 dataset with varying  $\alpha$  (blue) and  $\beta$  (red) values,  $\alpha/\beta = [0.001, 0.005, 0.006, 0.009, 0.01, 0.015, 0.020, 0.025, 0.03, 0.04, 0.05]$ . Test accuracy is the highest when  $\alpha$  and  $\beta$  equals 0.5.

In our experiments across various datasets and architectures, we found that a value of  $1e-3$  for the hyperparameters yields satisfactory results. This includes architectures ranging from ResNet-50 to Vision Transformers (ViT-Base), and datasets ranging from MNIST ( $\approx 60,000$  images of 10 classes) to ImageNet ( $\approx 1.1M$  images of 1000 classes). While conducting a parameter search for each dataset could potentially lead to further optimization, it’s worth noting that, in many cases, this step can be omitted without sacrificing performance significantly. For further optimization one can, of course, perform a tailored parameter search per dataset, but this is not quite necessary.

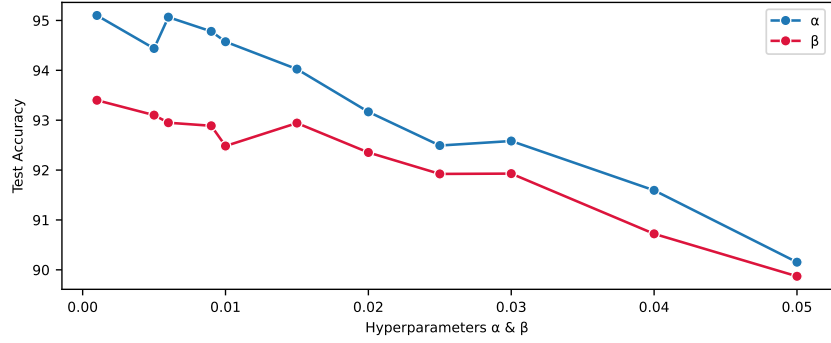


Figure 24: Test accuracies of RS-NN on different values of hyperparameters  $\alpha$  and  $\beta$  in the loss function.

### D.5.6 Ablation Study on the number of focal sets

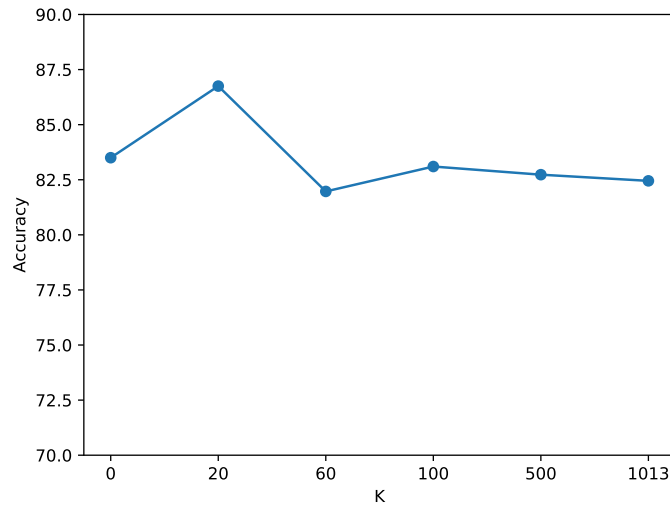


Figure 25: Ablation study on number of non-singleton focal sets  $K$  on CIFAR-10 dataset using ViT-Base. The maximum value of  $K$  can be 1013 for 10 classes (after excluding the singletons and empty set).

The number of non-singleton focal sets  $K$  to be budgeted is a hyperparameter and needs to be studied. A smaller value of  $K$  can lead to more similar results to classical classification while a larger value of  $K$  can increase the complexity. Therefore, we conducted an ablation study on the  $K$  on the CIFAR-10 dataset. It was found that a small value of  $K$  (comparable to the number of classes) works best and even performs better than  $K = 0$  (when there are no non-singleton focal sets) (see Fig. 25). Hence, using set prediction along with the proposed budgeting algorithm not only helps induce uncertainty quantification but also improves the performance of the model. Note that performance comparison was made in terms of accuracy. Smet’s Pignistic Transform [96] was used to compute class-wise probabilities from the predicted belief function. Fig. 25 shows an ablation study on different number of focal sets  $K$  for CIFAR-10 on the Vision-Transformer (ViT-Base) model.